Thin–Walled Structures 216 (2025) 113679

Contents lists available at ScienceDirect

Thin-Walled Structures

journal homepage: www.elsevier.com/locate/tws

Full length article

Free vibration of orthotropic rectangular mindlin plates via spectral element model under arbitrary boundary conditions

Yunlai Zhou [a], Feng Yao [a], Yubo Wang [a], Chunyu Bai [b], Shijie Liu [a], Magd Abdel Wahab [c,d,e,*]

[a] State Key Laboratory for Strength and Vibration of Mechanical Structures, School of Aerospace Engineering, Xi'an Jiaotong University, PR China
[b] Aircraft Strength Research Institute of China, National Key Laboratory of Strength and Structural Integrity 710065 Xi'an, PR China
[c] Soete Laboratory, Department of Electrical Energy, Metals, Mechanical Constructions, and Systems, Faculty of Engineering and Architecture, Ghent University, Belgium
[d] Parallel and Distributed Systems Laboratory, Jožef Stefan Institute, Jamova Cesta 39 SI-1000 Ljubljana, Slovenia
[e] College of Engineering, Yuan Ze University, Taiwan

ARTICLE INFO

Keywords:
Spectral element method
Orthotropic rectangular mindlin plates
Free Vibration
Arbitrary Boundary Conditions

ABSTRACT

This study proposes a novel spectral element model and introduces free vibration study of orthotropic rectangular Mindlin plates under arbitrary boundary conditions. Firstly, the general solution and boundary functions of the orthotropic rectangular Mindlin plate element are introduced in frequency domain with spectral form. Secondly, via the orthogonality of trigonometric functions, the spectral coefficients of the general solution are related to those of the boundary functions. Next, the spectral element matrix in terms of each plate element is derived from the force-displacement relation. Finally, the application of the spectral element model in free-vibration analysis is described in detail. Comparative study is further employed to affirm the reliability as well as the precision of the proposed spectral element model for rectangular Mindlin plates, including the spectral element method for isotropic plates, the Dynamic Stiffness Method (DSM) for orthotropic plates, and the Finite Element Method (FEM) for both plates.

1. Introduction

Orthotropic materials hold a significant position in modern engineering fields and are extensively employed in critical industries such as automotive manufacturing, naval engineering, and civil construction [1,2]. These materials exhibit different mechanical properties in three mutually perpendicular directions, making them an ideal choice for optimizing structural design and enhancing overall performance. Compared to isotropic materials, orthotropic materials better meet the mechanical demands of complex structures in various directions, thereby significantly improving the reliability and service life of engineering components. As fundamental structural elements, orthotropic plates are extensively used in aerospace, automotive, and shipbuilding sectors. Advanced composite laminated plates, due to their excellent mechanical properties, such as higher in-plane Young's modulus and transverse shear modulus, demonstrate superior performance compared to single-layer and isotropic laminated plates. Certain composites have superior strength-to-weight and stiffness-to-weight ratios, which renders them highly advantageous in engineering applications [3–6].

The free vibration of plates has consistently been a research hotspot, with current main methods including Finite Element Method (FEM), Dynamic Stiffness Method (DSM), and Spectral Element Method (SEM) [7,8]. FEM is widely used in structural analysis, primarily due to its applicability to structures with complex geometries. FEM uses frequency-independent polynomials as interpolation functions, requiring mesh refinement to improve computational accuracy. This is especially true in high-frequency ranges, where it results in an augmentation of the amount of degrees of freedom, thereby significantly raising computational costs [9–12]. DSM employs frequency-dependent shape functions as interpolation functions. Its core lies in utilizing free wave solutions and representing the structural vibration modes through infinite trigonometric series, which allows for accurately satisfying the plate's governing differential equations and providing high-precision solutions suitable for high-frequency vibration analysis [13–17]. However, DSM typically represents boundary conditions through infinite trigonometric series, making it impossible to directly apply the Fast Fourier Transform (FFT) algorithm for spectral analysis and vibration response simulation. This necessitates additional post-processing steps, increasing computational complexity [8]. Recently, deep learning methods have gradually demonstrated their potential in the free

* Corresponding author.
E-mail address: magd.abdelwahab@ugent.be (M. Abdel Wahab).

https://doi.org/10.1016/j.tws.2025.113679
Received 22 January 2025; Received in revised form 30 March 2025; Accepted 6 July 2025
Available online 10 July 2025

vibration analysis of plates [18–20]. Their core idea is to convert the partial differential equations that need to be solved and the boundary conditions into a loss function, and then approximate the displacement field of the plate or other physical quantities by training a deep neural network. Compared with traditional methods, the characteristic lies in being grid-free, without the need to construct an explicit element mesh or write a dedicated interpolation function form, and automatic differentiation can be used to compute high-order derivatives at scattered points, thereby satisfying the continuity requirements of high-order governing equations. However, deep learning methods require substantial computational resources for training and are prone to falling into local optima.

For orthotropic rectangular thin plates, Kshirsagar et al. [21] assessed the free vibration properties for orthotropic rectangular plates when subjected to random combinations of traditional boundary conditions, including clamped, simply supported, and so on. This study employed the superposition method as a theoretical framework. Xing et al. [22] proposed a novel separation of variables method, successfully deriving the accurate free vibration results for orthotropic thin plates with combinations of simply supported and clamped boundary conditions. Liu et al. [23,24] developed the spectral DSM (S-DSM), a pioneering method to the precise free vibration study of general orthotropic composite plates. This method ingeniously integrates the strengths of the classical DSM with those of spectral methods, emulating the synergy seen in FEM and boundary element method. Ghorbel et al. [25] utilized the DSM to study the free vibration of orthotropic Kirchhoff plates. Certain method is grounded in the strong form of the Kirchhoff plate equations and series solution methods, leveraging the symmetry of plate free boundary conditions and Gorman-type decomposition techniques to derive the dynamic stiffness matrix. This facilitates efficient matrix assembly. For complex plate systems assembled from multiple orthotropic rectangular thin plates, Wang et al. [26] extended the applicability of the separation of variables method and proposed an extended separation of variables approach. Using the Rayleigh principle and an improved multi-boundary compatibility technique, they first assumed that the eigenfunctions in the respective coordinate directions of each subplate are separable. Then, displacement continuity and internal force equilibrium conditions are imposed at the junctions, and finally, a closed-form eigenvalue solution is obtained under the governing equations of the orthotropic materials. Papkov et al. [27] developed DSM applicable to both isotropic and orthotropic rectangular plates, capable of integrating the dynamic stiffness characteristics of plates with those of other components such as rods and beams. For the first time, this method was combined with FEM. The method involves the introduction of Fourier coefficients, which enable the representation of force-displacement relationships at each plate node, thus deriving the dynamic stiffness matrices for isotropic, and orthotropic plates as well.

The fundamental theory of thick plates is initially proposed by Reissner [28], primarily for solving static problems, then is subsequently expanded to the dynamic field by Mindlin [29]. In comparison with the Kirchhoff plate theory, the Mindlin plate theory takes certain effects of shear deformation and rotary inertia into account. Kshirsagar et al. [30] proposed a non-truncated infinite series superposition method. Based on the traditional superposition method, they introduced double or multiple Fourier series expansions in the displacement field and used

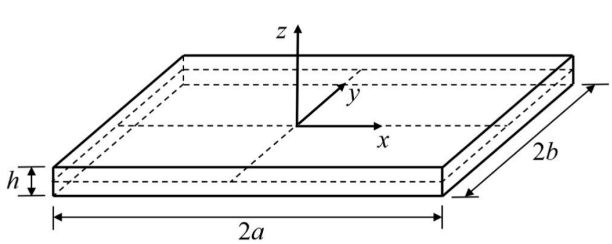

Fig. 1. A rectangular plate.

mathematical software for precise series summation processing. This method achieved high-precision theoretical analysis for various boundary conditions, (including buckling and vibration of anisotropic plates), avoiding the extensive and complex derivations of closed-form Levy or Navier solutions when material orthotropy and thickness shear effects are introduced. Shi et al. [31] adopted an energy variational method based on an improved Fourier series expansion and the Rayleigh–Ritz method. They represented the plate's deflection and rotational components using a novel trigonometric series, simulated arbitrary boundary conditions with elastic boundary springs, and then constructed an energy functional by treating all Fourier coefficients as generalized coordinates. Finally, the problem was transformed into a standard matrix eigenvalue problem to solve for natural frequencies and mode shapes. Bahrami et al. [32], based on Levy-type boundary assumptions, used a frequency domain spectral element method for the free and forced vibration analysis of moderately thick orthotropic rectangular plates. In their study, a Fourier series expansion was employed in one direction of the plate, reducing the two-dimensional problem to one dimension, which enabled the construction of a spectral stiffness matrix. Liu and Xing [33,34] derived precise closed-form solutions for the free vibration of orthotropic rectangular Mindlin plates by employing the variables separation method. Based on Mindlin plate theory, Papkov and Banerjee [35] proposed dynamic stiffness formulas for analyzing thick orthotropic rectangular plates. By using modified trigonometric bases, the solution of the plate free vibration was constructed. This system established a connection between certain Fourier coefficients at the four edges of such plate and the boundary conditions for the motion. By linking the displacement vector with the force vector, they further derived the force-displacement relations.

SEM is a numerical analysis method that integrates FEM, DSM, and spectral method [36–38]. Early research on spectral element modeling of plate elements mainly focused on Levy-type plates. Doyle [39] was the first to derive the spectral element for Levy-type plates, laying the foundation for the subsequent development of spectral plate elements. Later, Campos and Arruda [40] proposed a SEM for plate elements applicable to arbitrary boundary conditions. However, in this method the boundary functions are expressed in the spatial domain using trigonometric series, which makes it impossible to directly compute the spectral coefficients with the FFT algorithm, thereby limiting the efficiency of the method. In the book *Spectral Element Method in Structural Dynamics*, Lee [36] also derived the spectral element model for Levy-type plates in detail. In 2016, Park et al. [10,41] combined the boundary splitting method with the spectral super element method to construct a spectral element matrix for rectangular finite plates under arbitrary boundary conditions. Nevertheless, the approximate general solution obtained by the finite strip element method does not completely satisfy the homogeneous governing differential equations, so the accuracy and convergence of this model are inferior to those of the dynamic stiffness model obtained directly from the homogeneous equations. Recently, Kim and Lee [8,42] achieved accurate spectral element modeling for rectangular Kirchhoff and Mindlin plates under arbitrary boundary conditions. They derived the general solution for rectangular plate elements and the spectral representation of the boundary functions in the frequency domain, used the projection method to correlate the spectral coefficients, and constructed the spectral element matrix based on the force–displacement relationship. Zhou et al. [43] utilized this model to investigate the vibration of bandgap features of periodic plates, further verifying the high accuracy of this method.

With the spectral element modeling method introduced by Kim and Lee, this study constructs a spectral element model suitable for orthotropic rectangular Mindlin plates under arbitrary boundary conditions. It derives the general solution of orthotropic rectangular plate elements and the spectral representations of boundary functions in the frequency domain, employs the projection method to associate spectral coefficients, and constructs the spectral element matrix via the force-displacement relation. The derived spectral element model is applied to the solutions of isotropic and orthotropic plates, and a comparison with previous studies is made to verify the feasibility of this study.

2. Spectral element model

2.1. Vibration equation

Fig. 1 illustrates a thick rectangular plate with a length of $2a$, a width of $2b$, and a thickness of h. With the principles of Mindlin plate theory, the displacement field of the plate is postulated as follows [33]:

$$\begin{aligned} w &= w(x,y,z,t) \\ u &= -z\phi_x(x,y,z,t) \\ v &= -z\phi_y(x,y,z,t) \end{aligned} \tag{1}$$

where w represents the transverse displacement at the mid-plane of the plate; ϕ_x and ϕ_y denote the rotations about the x-axis and y-axis, respectively; and z means the coordinate in the thickness direction, ranging from $-h/2 \le z \le h/2$.

The following is a summary of the geometric and normal boundary conditions to the orthotropic rectangular Mindlin plate, and which are located at the plate's four edges:

$$\begin{aligned} & w(x,-b) = w_o^B(x) \text{ or } -Q_y(x,-b) = Q_{oy}^B(x) \\ & \phi_x(x,-b) = \phi_{ox}^B(x) \text{ or } M_{xy}(x,-b) = M_{oxy}^B(x) \\ & \phi_y(x,-b) = \phi_{oy}^B(x) \text{ or } M_y(x,-b) = M_{oy}^B(x) \\ & w(x,b) = w_o^U(x) \text{ or } Q_y(x,b) = Q_{oy}^U(x) \\ & \phi_x(x,b) = \phi_{ox}^U(x) \text{ or } -M_{xy}(x,b) = M_{oxy}^U(x) \\ & \phi_y(x,b) = \phi_{oy}^U(x) \text{ or } -M_y(x,b) = M_{oy}^U(x) \\ & w(-a,y) = w_o^L(y) \text{ or } -Q_x(-a,y) = Q_{ox}^L(y) \\ & \phi_x(-a,y) = \phi_{ox}^L(y) \text{ or } M_x(-a,y) = M_{ox}^L(y) \\ & \phi_y(-a,y) = \phi_{oy}^L(y) \text{ or } M_{xy}(-a,y) = M_{oxy}^L(y) \\ & w(a,y) = w_o^R(y) \text{ or } Q_x(a,y) = Q_{ox}^R(y) \\ & \phi_x(a,y) = \phi_{ox}^R(y) \text{ or } -M_x(a,y) = M_{ox}^R(y) \\ & \phi_y(a,y) = \phi_{oy}^R(y) \text{ or } -M_{xy}(a,y) = M_{oxy}^R(y) \end{aligned} \tag{2}$$

where Q_x and Q_y mean the transverse shear forces, respectively, i.e.:

$$Q_y = C_{44}\left(\frac{\partial w}{\partial y} - \phi_y\right),\ Q_x = C_{55}\left(\frac{\partial w}{\partial x} - \phi_x\right), \tag{3}$$

M_x and M_y represent the resultant bending moments and are defined as:

$$M_x = -\left(D_{11}\frac{\partial \phi_x}{\partial x} + D_{12}\frac{\partial \phi_y}{\partial y}\right),\ M_y = -\left(D_{22}\frac{\partial \phi_y}{\partial y} + D_{21}\frac{\partial \phi_x}{\partial x}\right) \tag{4}$$

and $M_{xy} = M_{yx}$ denote the resultant twisting moments, are expressed as:

$$M_{xy} = -D_{66}\left(\frac{\partial \phi_x}{\partial y} + \frac{\partial \phi_y}{\partial x}\right) \tag{5}$$

In Eqs. (3), (4), and (5), the bending stiffness and shear stiffness constants are:

$$\begin{aligned} & D_{11} = \frac{E_{xy}h^3}{12(1-\nu_{xy}\nu_{yx})}, D_{12} = \frac{\nu_{yx}E_{xy}h^3}{12(1-\nu_x\nu_y)}, \\ & D_{22} = \frac{E_{yx}h^3}{12(1-\nu_{xy}\nu_{yx})}, D_{21} = \frac{\nu_{xy}E_{yx}h^3}{12(1-\nu_{xy}\nu_{yx})}, \\ & D_{66} = \frac{G_{xy}h^3}{12}, C_{44} = \kappa G_{yz}h, C_{55} = \kappa G_{xz}h \end{aligned} \tag{6}$$

where κ denotes the shear correction factor, $\nu_{yx}E_{xy} = \nu_{xy}E_{yx}$, $D_{12} = D_{21}$.

Based on dynamic equilibrium and considering the transverse force and the equilibrium moment, the vibration equation is established. The transverse equilibrium equation is:

$$\frac{\partial Q_x}{\partial x} + \frac{\partial Q_y}{\partial y} - \rho h\frac{\partial^2 w}{\partial t^2} = 0, \tag{7}$$

The rotational equilibrium about the x-axis follows as:

$$-\frac{\partial M_x}{\partial x} - \frac{\partial M_{xy}}{\partial y} + Q_x - \frac{\rho h^3}{12}\frac{\partial^2 \phi_x}{\partial t^2} = 0, \tag{8}$$

The rotational equilibrium about the y-axis is given by:

$$-\frac{\partial M_{xy}}{\partial x} - \frac{\partial M_y}{\partial y} + Q_y - \frac{\rho h^3}{12}\frac{\partial^2 \phi_y}{\partial t^2} = 0, \tag{9}$$

where in Eqs. (7), (8) and (9), ρ is the density.

By substituting Eqs. (3), (4), and (5) into Eqs. (7), (8), and (9), the secondary governing equations for the orthotropic rectangular Mindlin plate are as follows:

$$\begin{aligned} & C_1\left(\frac{\partial^2 w}{\partial x^2} - \frac{\partial \phi_x}{\partial x}\right) + C_2\left(\frac{\partial^2 w}{\partial y^2} - \frac{\partial \phi_y}{\partial y}\right) + \Omega^4 w = 0 \\ & D_1\frac{\partial^2 \phi_x}{\partial x^2} + \frac{\partial^2 \phi_x}{\partial y^2} + D_3\frac{\partial^2 \phi_y}{\partial x \partial y} + C_1\left(\frac{\partial w}{\partial x} - \phi_x\right) + \Omega_h^4\phi_x = 0 \\ & D_2\frac{\partial^2 \phi_y}{\partial y^2} + \frac{\partial^2 \phi_y}{\partial x^2} + D_3\frac{\partial^2 \phi_x}{\partial x \partial y} + C_2\left(\frac{\partial w}{\partial y} - \phi_y\right) + \Omega_h^4\phi_y = 0 \end{aligned} \tag{10}$$

where

$$\begin{aligned} & D_1 = D_{11}/D_{66}, D_2 = D_{22}/D_{66}, D_3 = 1 + D_{12}/D_{66} \\ & C_1 = C_{55}/D_{66}, \quad C_2 = C_{44}/D_{66} \\ & \Omega_h^4 = \rho h^3\omega^2/12D_{66}, \Omega^4 = \rho h\omega^2/D_{66}. \end{aligned} \tag{11}$$

2.2. General solution in spectral form

The general solution of Eq. (10) is given in the following harmonic form:

$$\boldsymbol{w}(x,y) = \begin{Bmatrix} w(x,y) \\ \phi_x(x,y) \\ \phi_y(x,y) \end{Bmatrix} = \begin{Bmatrix} v_1 \\ v_2 \\ v_3 \end{Bmatrix} e^{i(k_x x + k_y y)} = \mathbf{v}e^{i(k_x x + k_y y)} \tag{12}$$

where $i = \sqrt{-1}$ is the imaginary unit, $\mathbf{v} = \{v_1, v_2, v_3\}^{\mathrm{T}}$ is a constant vector, and k_x and k_y are the wave numbers relative to the x and y coordinates. There are infinitely many values of k_x and k_y that comply with Eq. (10). The general solution can be written in the subsequent trigonometric series form [42]:

$$\boldsymbol{w}(x,y) = \boldsymbol{w}^{(x)}(x,y) + \boldsymbol{w}^{(y)}(x,y) \tag{13}$$

where

$$\begin{aligned} & \boldsymbol{w}^{(x)}(x,y) = \begin{Bmatrix} w^{(x)}(x,y) \\ \phi_x^{(x)}(x,y) \\ \phi_y^{(x)}(x,y) \end{Bmatrix} = \sum_{\infty}^{p=-\infty} \begin{Bmatrix} v_{p1}^{(x)} \\ v_{p2}^{(x)} \\ v_{p3}^{(x)} \end{Bmatrix} e^{i(k_{xp}x + K_{xp}y)} = \sum_{\infty}^{p=-\infty} \mathbf{v}_p^{(x)} e^{i(k_{xp}x + K_{xp}y)} \\ & \boldsymbol{w}^{(y)}(x,y) = \begin{Bmatrix} w^{(y)}(x,y) \\ \phi_x^{(y)}(x,y) \\ \phi_y^{(y)}(x,y) \end{Bmatrix} = \sum_{\infty}^{q=-\infty} \begin{Bmatrix} v_{q1}^{(y)} \\ v_{q2}^{(y)} \\ v_{q3}^{(y)} \end{Bmatrix} e^{i(K_{yq}x + k_{yq}y)} = \sum_{\infty}^{q=-\infty} \mathbf{v}_q^{(y)} e^{i(K_{yq}x + k_{yq}y)} \end{aligned} \tag{14}$$

where k_{xp} and k_{yq} denote discrete wavenumbers defined by:

$$\begin{aligned} & k_{xp} = p\Delta k_x, (p = 0, \pm 1, \pm 2, \pm 3, \ldots) \\ & k_{yq} = q\Delta k_y, (q = 0, \pm 1, \pm 2, \pm 3, \ldots) \end{aligned} \tag{15}$$

and

$$\Delta k_x = \frac{2\pi}{4a},\ \Delta k_y = \frac{2\pi}{4b} \tag{16}$$

Substituting $\boldsymbol{w}^{(x)}(x, y)$ and $\boldsymbol{w}^{(y)}(x, y)$ from Eq. (14) into Eq. (10), yields:

$$\begin{aligned} &\mathbf{M}_p^{(x)}\mathbf{v}_p^{(x)} = 0, (p = 0, \pm 1, \pm 2, \pm 3, \ldots) \\ &\mathbf{M}_q^{(y)}\mathbf{v}_q^{(y)} = 0, (q = 0, \pm 1, \pm 2, \pm 3, \ldots) \end{aligned} \tag{17}$$

$$\mathbf{M}_p^{(x)} = \begin{bmatrix} -C_2K_{xp}^2 + \Omega^4 - C_1{k_{xp}}^2 & -C_1k_{xp}\mathrm{i} & -C_2K_{xp}\mathrm{i} \\ C_1k_{xp}\mathrm{i} & -K_{xp}^2 + \Omega_h^4 - D_1{k_{xp}}^2 - C_1 & -D_3K_{xp}k_{xp} \\ C_2K_{xp}\mathrm{i} & -D_3K_{xp}k_{xp} & -D_2K_{xp}^2 + \Omega_h^4 - {k_{xp}}^2 - C_2 \end{bmatrix}$$

$$\mathbf{M}_q^{(y)} = \begin{bmatrix} -C_1K_{yq}^2 + \Omega^4 - C_2{k_{yq}}^2 & -C_1K_{yq}\mathrm{i} & -C_2k_{yq}\mathrm{i} \\ C_1K_{yq}\mathrm{i} & -D_1K_{yq}^2 + \Omega_h^4 - {k_{yq}}^2 - C_1 & -D_3K_{yq}k_{yq} \\ C_2k_{yq}\mathrm{i} & -D_3K_{yq}k_{yq} & -K_{yq}^2 + \Omega_h^4 - D_2{k_{yq}}^2 - C_2 \end{bmatrix} \tag{18}$$

In Eq. (18), by setting $\det\left(\mathbf{M}_p^{(x)}\right) = 0$ and $\det\left(\mathbf{M}_q^{(y)}\right) = 0$, we can solve for K_{xp} and K_{yq}. The values of K_{xp} and K_{yq} obtained in MATLAB are presented in the form of the roots of a cubic polynomial equation as follows:

$$\begin{aligned} &\vartheta_x z_x^3 + \iota_x z_x^2 + \tau_x z_x + \delta_x = 0 \\ &\vartheta_y z_y^3 + \iota_y z_y^2 + \tau_y z_y + \delta_y = 0 \end{aligned} \tag{19}$$

where

$$\begin{aligned} K_{xp} &= \pm\sqrt{z_x} \\ K_{yq} &= \pm\sqrt{z_y} \end{aligned} \tag{20}$$

$$\begin{gathered} \vartheta_x = C_2D_2 \\ \iota_x = C_2k_{xp}^2 - D_2\Omega^4 - C_2\Omega_h^4 + C_1D_2k_{xp}^2 + C_1C_2D_2 - C_2D_3^2k_{xp}^2 - C_2D_2\Omega_h^4 + C_2D_1D_2k_{xp}^2 \\ \tau_x = C_2\Omega_h^8 - C_2\Omega^4 - \Omega^4k_{xp}^2 + \Omega^4\Omega_h^4 + C_1k_{xp}^4 + D_2\Omega^4\Omega_h^4 + 2C_1C_2k_{xp}^2 + C_2D_1k_{xp}^4 \\ -C_1D_3^2k_{xp}^4 - C_1\Omega_h^4k_{xp}^2 - C_2\Omega_h^4k_{xp}^2 - C_1C_2\Omega_h^4 - C_1D_2\Omega^4 + D_3^2\Omega^4k_{xp}^2 + 2C_1C_2D_3k_{xp}^2 \\ +C_1D_1D_2k_{xp}^4 - C_1D_2\Omega_h^4k_{xp}^2 - C_2D_1\Omega_h^4k_{xp}^2 - D_1D_2\Omega^4k_{xp}^2 \\ \delta_x = C_1\Omega^4\Omega_h^4 - \Omega^4\Omega_h^8 + C_2\Omega^4\Omega_h^4 + C_1D_1k_{xp}^6 - C_1\Omega^4k_{xp}^2 - C_1\Omega_h^4k_{xp}^4 + C_1\Omega_h^8k_{xp}^2 \\ -D_1\Omega^4k_{xp}^4 - C_1C_2\Omega^4 + \Omega^4\Omega_h^4k_{xp}^2 + D_1\Omega^4\Omega_h^4k_{xp}^2 + C_1C_2D_1k_{xp}^4 - C_1C_2\Omega_h^4k_{xp}^2 \\ -C_2D_1\Omega^4k_{xp}^2 - C_1D_1\Omega_h^4k_{xp}^4 \end{gathered} \tag{21}$$

$$\begin{gathered} \vartheta_y = C_1D_1 \\ \iota_y = C_1k_{yq}^2 - D_1\Omega^4 - C_1\Omega_h^4 + C_2D_1k_{yq}^2 + C_1C_2D_1 - C_1D_3^2k_{yq}^2 - C_1D_1\Omega_h^4 + C_1D_1D_2k_{yq}^2 \\ \tau_y = C_1\Omega_h^8 - C_1\Omega^4 - \Omega^4k_{yq}^2 + \Omega^4\Omega_h^4 + C_2k_{yq}^4 + D_1\Omega^4\Omega_h^4 + 2C_1C_2k_{yq}^2 + C_1D_2k_{yq}^4 \\ -C_2D_3^2k_{yq}^4 - C_1\Omega_h^4k_{yq}^2 - C_2\Omega_h^4k_{yq}^2 - C_1C_2\Omega_h^4 - C_2D_1\Omega^4 + D_3^2\Omega^4k_{yq}^2 + 2C_1C_2D_3k_{yq}^2 \\ +C_2D_1D_2k_{yq}^4 - C_1D_2\Omega_h^4k_{yq}^2 - C_2D_1\Omega_h^4k_{yq}^2 - D_1D_2\Omega^4k_{yq}^2 \\ \delta_y = C_1\Omega^4\Omega_h^4 - \Omega^4\Omega_h^8 + C_2\Omega^4\Omega_h^4 + C_2D_2k_{yq}^6 - C_2\Omega^4k_{yq}^2 - C_2\Omega_h^4k_{yq}^4 + C_2\Omega_h^8k_{yq}^2 \\ -D_2\Omega^4k_{yq}^4 - C_1C_2\Omega^4 + \Omega^4\Omega_h^4k_{yq}^2 + D_2\Omega^4\Omega_h^4k_{yq}^2 + C_1C_2D_2k_{yq}^4 - C_1C_2\Omega_h^4k_{yq}^2 \\ -C_1D_2\Omega^4k_{yq}^2 - C_2D_2\Omega_h^4k_{yq}^4 \end{gathered} \tag{22}$$

Eq. (19) is a cubic equation, which can be solved using Cordano formulas. By substituting the solutions into Eq. (20), the values of K_{xp} and K_{yq} can be obtained, where K_{xp} and K_{yq} each have 6 roots.

By substituting $K_{xp(j)}$ and $K_{yq(j)}$ (where $j = 1\sim6$) into Eq. (18), the corresponding eigenvectors $\mathbf{v}_{p(j)}^{(x)} = \left\{v_{p1(j)}^{(x)}, v_{p2(j)}^{(x)}, v_{p3(j)}^{(x)}\right\}^{\mathrm{T}}$ and $\mathbf{v}_{q(j)}^{(y)} = \left\{v_{q1(j)}^{(y)}, v_{q2(j)}^{(y)}, v_{q3(j)}^{(y)}\right\}^{\mathrm{T}}$ can be obtained.

Using the ratio form of the components of the eigenvectors, Eq. (14) becomes:

$$\boldsymbol{w}^{(x)}(x,y) = \sum_{\infty}^{p=-\infty} \frac{1}{\sqrt{lpa}} \left(\sum_{4}^{j=1} \mathrm{e}^{\mathrm{i}K_{xp(j)}y - \mathrm{i}R_{xp(j)}b} \begin{Bmatrix} 1 \\ \dfrac{v_{p2(j)}^{(x)}}{v_{p1(j)}^{(x)}} \\ \dfrac{v_{p3(j)}^{(x)}}{v_{p1(j)}^{(x)}} \end{Bmatrix} v_{p1(j)}^{(x)} + \sum_{6}^{j=5} \mathrm{e}^{\mathrm{i}K_{xp(j)}y - \mathrm{i}R_{xp(j)}^{b}} \begin{Bmatrix} 0 \\ 1 \\ \dfrac{v_{p3(j)}^{(x)}}{v_{p2(j)}^{(x)}} \end{Bmatrix} v_{p2(j)}^{(x)} \right) \mathrm{e}^{\mathrm{i}k_{xp}x}$$

$$\boldsymbol{w}^{(y)}(x,y) = \sum_{\infty}^{q=-\infty} \frac{1}{\sqrt{\zeta q^b}} \left(\sum_{4}^{j=1} \mathrm{e}^{\mathrm{i}K_{yq(j)}x - \mathrm{i}R_{yq(j)}a} \begin{Bmatrix} 1 \\ \dfrac{v_{q2(j)}^{(0)}}{v_{q1(j)}^{(0)}} \\ \dfrac{v_{q3(j)}^{(0)}}{v_{q1(j)}^{(D)}} \end{Bmatrix} v_{q1(j)}^{(y)} + \sum_{6}^{j=5} \mathrm{e}^{\mathrm{i}K_{yq(j)}x - \mathrm{i}R_{yq(j)}a} \begin{Bmatrix} 0 \\ 1 \\ \dfrac{v_{q3(j)}^{(y)}}{v_{q2(j)}^{(y)}} \end{Bmatrix} v_{q2(j)}^{(y)} \right) \mathrm{e}^{\mathrm{i}k_{yq}y} \tag{23}$$

which can be simplified as:

$$\boldsymbol{w}^{(x)}(x,y) = \mathrm{X}\mathbf{Z}^{(x)}(x,y), \boldsymbol{w}^{(y)}(x,y) = \mathrm{X}\mathbf{Z}^{(y)}(x,y) \tag{24}$$

where

$$\mathrm{X} = \begin{bmatrix} 1 & 0 & 0 & 0 & 0 \\ 0 & 1 & 0 & 1 & 0 \\ 0 & 0 & 1 & 0 & 1 \end{bmatrix} \tag{25}$$

$$\mathbf{Z}^{(x)}(x,y) = \sum_{p=-\infty}^{\infty} \mathbf{z}_p^{(x)}(y) \begin{Bmatrix} \widehat{\mathbf{v}}_{p1}^{(x)} \\ \widehat{\mathbf{v}}_{p2}^{(x)} \end{Bmatrix} \mathrm{e}^{\mathrm{i}k_{xp}x},\ \mathbf{Z}^{(y)}(x,y) = \sum_{q=-\infty}^{\infty} \mathbf{z}_q^{(y)}(x) \begin{Bmatrix} \widehat{\mathbf{v}}_{q1}^{(y)} \\ \widehat{\mathbf{v}}_{q2}^{(y)} \end{Bmatrix} \mathrm{e}^{\mathrm{i}k_{yq}y} \tag{26}$$

The function definitions in Eq. (26) can be found in Appendix A.

Applying Euler's formula to Eq. (26) and combining the symmetry in the positive and negative directions, an infinite trigonometric series form is obtained. Subsequently, utilizing the orthogonality of Fourier series, the displacements and rotations are decomposed into a series of sine and cosine functions. Since the boundary conditions require the rotations and displacements at the plate boundaries to be zero, imposing constraints on certain coefficients in the series and eliminating terms that do not satisfy the boundary conditions. Following this, the coefficient matrix of the Fourier series is introduced, and by setting the distribution of odd and even coefficients, it is ensured that each term of the results satisfies the dynamic equations as well as boundary conditions. For the convenience of further numerical processing, the orthogonal trigonometric series form is converted into an exponential Fourier series form using Euler's formula. The cosine and sine functions are expressed in terms of complex exponentials, thereby uniformly representing the orthogonal trigonometric functions as:

$$\begin{aligned} &\cos(k_{xp}x) = \frac{\mathrm{e}^{\mathrm{i}k_{xp}x} + \mathrm{e}^{-\mathrm{i}k_{xp}x}}{2}, \sin(k_{xp}x) = \frac{\mathrm{e}^{\mathrm{i}k_{xp}x} - \mathrm{e}^{-\mathrm{i}k_{xp}x}}{2\mathrm{i}} \\ &\cos(k_{yq}y) = \frac{\mathrm{e}^{\mathrm{i}k_{yq}y} + \mathrm{e}^{-\mathrm{i}k_{yq}y}}{2}, \sin(k_{yq}y) = \frac{\mathrm{e}^{\mathrm{i}k_{yq}y} - \mathrm{e}^{-\mathrm{i}k_{yq}y}}{2\mathrm{i}} \end{aligned} \tag{27}$$

The solutions for the rectangular plate, $\mathbf{Z}^{(x)}(x, y)$ and $\mathbf{Z}^{(y)}(x, y)$ can be rewritten in the form of an infinite Fourier series as:

$$\mathbf{Z}^{(x)}(x,y) = \sum_{p=-\infty}^{\infty} \widetilde{\mathbf{Z}}_p^{(x)}(y)\mathrm{e}^{\mathrm{i}k_{xp}x}, \mathbf{Z}^{(y)}(x,y) = \sum_{q=-\infty}^{\infty} \widetilde{\mathbf{Z}}_q^{(y)}(x)\mathrm{e}^{\mathrm{i}k_{yq}y} \tag{28}$$

where

$$\widetilde{\mathbf{z}}_p^{(x)}(y) = \mathbf{z}_p^{(x)}(y) \begin{Bmatrix} \overline{\mathbf{v}}_{p1}^{(x)} \\ \overline{\mathbf{v}}_{p2}^{(x)} \end{Bmatrix}, \widetilde{\mathbf{z}}_q^{(y)}(x) = \mathbf{z}_q^{(y)}(x) \begin{Bmatrix} \overline{\mathbf{v}}_{q1}^{(y)} \\ \overline{\mathbf{v}}_{q2}^{(y)} \end{Bmatrix} \tag{29}$$

$$\hat{\mathbf{v}}^{(x)}_{(-p)1} = \begin{cases} \overline{\mathbf{v}}^{(x)}_{p1} & \text{if } p = 0,2,4,\ldots \\ -\overline{\mathbf{v}}^{(x)}_{p1} & \text{if } p = 1,3,5,\ldots \end{cases}, \hat{\mathbf{v}}^{(x)}_{(-p)2} = \begin{cases} -\overline{\mathbf{v}}^{(x)}_{p2} & \text{if } p = 0,2,4,\ldots \\ \overline{\mathbf{v}}^{(x)}_{p2} & \text{if } p = 1,3,5,\ldots \end{cases}$$
$$\hat{\mathbf{v}}^{(y)}_{(-q)1} = \begin{cases} \overline{\mathbf{v}}^{(y)}_{q1} & \text{if } q = 0,2,4,\ldots \\ -\overline{\mathbf{v}}^{(y)}_{q1} & \text{if } q = 1,3,5,\ldots \end{cases}, \hat{\mathbf{v}}^{(y)}_{(-q)2} = \begin{cases} -\overline{\mathbf{v}}^{(y)}_{q2} & \text{if } q = 0,2,4,\ldots \\ \overline{\mathbf{v}}^{(y)}_{q2} & \text{if } q = 1,3,5,\ldots \end{cases} \tag{30}$$

In light of the infinite nature of the Fourier series, it is imperative that truncation is employed during practical computations. To achieve this, discrete sampling points N_x and N_y are defined, and the truncated infinite exponential Fourier series is given as follows:

$$\mathbf{Z}^{(x)}(x,y) = \frac{1}{N_x}\sum_{\frac{N_x}{2}1}^{p=\frac{N_x}{2}} \overline{\mathbf{Z}}^{(x)}_p(y)\mathrm{e}^{\mathrm{i}k_{xp}x}, \mathbf{Z}^{(y)}(x,y) = \frac{1}{N_y}\sum_{\frac{N_y}{2}-1}^{q=\frac{N_y}{2}} \overline{\mathbf{Z}}^{(y)}_q(x)\mathrm{e}^{\mathrm{i}k_{yq}y} \tag{31}$$

where $\overline{\mathbf{z}}^{(x)}_p(y)$ and $\overline{\mathbf{Z}}^{(y)}_q(x)$ denote the spatial domain frequency components:

$$\overline{\mathbf{Z}}^{(x)}_p(y) = N_x\widetilde{\mathbf{Z}}^{(x)}_p(y), \overline{\mathbf{Z}}^{(y)}_q(x) = N_y\widetilde{\mathbf{Z}}^{(y)}_q(x) \tag{32}$$

N_x and N_y mean the amount of sampling points along the x and y coordinates, respectively:

$$N_x = 4a/\Delta x,\ N_y = 4b/\Delta y \tag{33}$$

By substituting Eq. (31) into Eq. (24), hereinafter substituting the results into Eq. (13), the general solution is obtained as:

$$\boldsymbol{w}(x,y) = \mathbf{X}\left(\frac{1}{N_x}\sum_{\frac{N_x}{2}-1}^{p=\frac{N_x}{2}} \overline{\mathbf{Z}}^{(x)}_p(y)\mathrm{e}^{\mathrm{i}k_{xp}x} + \frac{1}{N_y}\sum_{\frac{N_y}{2}-1}^{q=-\frac{N_y}{2}} \overline{\mathbf{Z}}^{(y)}_q(x)\mathrm{e}^{\mathrm{i}k_{yq}y}\right) \tag{34}$$

2.3. Boundary conditions

To apply SEM, the boundary conditions have to be transformed into vector form. In the x-direction, the boundary conditions have the following expressions:

$$\begin{aligned} \mathbf{d}^{(x)}_{o1}(x) &= \left\{w^B_o(x), w^U_o(x), \phi^B_{oy}(x), \phi^U_{oy}(x)\right\}^{\mathrm{T}} \\ \mathbf{d}^{(x)}_{o2}(x) &= \left\{\phi^B_{ox}(x), \phi^U_{ox}(x)\right\}^{\mathrm{T}} \\ \mathbf{f}^{(x)}_{o1}(x) &= \left\{Q^B_{oy}(x), Q^U_{oy}(x), M^B_{oy}(x), M^U_{oy}(x)\right\}^{\mathrm{T}}(-a \le x \le a) \\ \mathbf{f}^{(x)}_{o2}(x) &= \left\{M^B_{oxy}(x), M^U_{oxy}(x)\right\}^{\mathrm{T}} \end{aligned} \tag{35}$$

In the y-direction, the boundary conditions have the following expressions:

$$\begin{aligned} \mathbf{d}^{(y)}_{o1}(y) &= \left\{w^L_o(y),\quad w^R_o(y),\quad \phi^L_{ox}(y),\quad \phi^R_{ox}(y)\right\}^{\mathrm{T}} \\ \mathbf{d}^{y)}_{o2}(y) &= \left\{\phi^L_{oy}(y),\quad \phi^R_{oy}(y)\right\}^{\mathrm{T}} \\ \mathbf{f}^{(y)}_{o1}(y) &= \left\{Q^L_{ox}(y),\quad Q^R_{ox}(y), M^L_{ox}(y),\quad M^R_{ox}(y)\right\}^{\mathrm{T}}(-b \le y \le b) \\ \mathbf{f}^{(y)}_{o2}(y) &= \left\{M^L_{oxy}(y),\quad M^R_{oxy},(y)\right\}^{\mathrm{T}} \end{aligned} \tag{36}$$

2.4. Spectral element formulation

In real engineering applications, the boundary functions sometimes do not have periodic features within the initial spatial domain ($x \in [-a,a]$ and $y \in [-b,b]$). To avoid the leakage error, the boundary functions are transformed to be periodic and expressed within the extended spatial domain ($x \in [-2a,2a]$ and $y \in [-2b,2b]$). Using Discrete Fourier Transform (DFT), the boundary functions can be converted into the following spectral form:

$$\begin{aligned} \begin{Bmatrix} \mathbf{d}^{(\alpha)}_1(\alpha) \\ \mathbf{f}^{(\alpha)}_1(\alpha) \end{Bmatrix} &= \frac{1}{N_\alpha}\sum_{\frac{N_\alpha}{2}-1}^{n=-N_\alpha/2} \begin{Bmatrix} \overline{\mathbf{d}}^{(\alpha)}_{n1} \\ \mathbf{f}^{(\alpha)}_{n1} \end{Bmatrix}\mathrm{e}^{\mathrm{i}k_{\alpha n}\alpha}, (-2l \le \alpha \le 2l) \\ \begin{Bmatrix} \mathbf{d}^{(\alpha)}_2(\alpha) \\ \mathbf{f}^{(\alpha)}_2(\alpha) \end{Bmatrix} &= \frac{1}{N_\alpha}\sum_{\frac{N_\alpha}{2}-1}^{n=-N_\alpha/2} \begin{Bmatrix} \overline{\mathbf{d}}^{(\alpha)}_{n2} \\ \mathbf{f}^{(\xi)}_{n2} \end{Bmatrix}\mathrm{e}^{\mathrm{i}k_{\alpha n}\alpha}, (-2l \le \alpha \le 2l) \end{aligned} \tag{37}$$

where the spectral components are specified as:

$$\begin{aligned} \mathbf{d}^{(\alpha)}_{n1} &= \left\{W^{(-)}_n, W^{(+)}_n, \phi^{(-)}_{n\beta}, \phi^{(+)}_{n\beta}\right\}^{\mathrm{T}} \\ \mathbf{f}^{(\alpha)}_{n1} &= \left\{Q^{(-)}_{n\beta}, Q^{(+)}_{n\beta}, M^{(-)}_{n\beta}, M^{(+)}_{n\beta}\right\}^{\mathrm{T}} \\ \mathbf{d}^{(\alpha)}_{n2} &= \left\{\phi^{(-)}_{n\alpha}, \phi^{(+)}_{n\alpha}\right\}^{\mathrm{T}} \\ \mathbf{f}^{(\alpha)}_{n2} &= \left\{M^{(-)}_{n\alpha\beta}, M^{(+)}_{n\alpha\beta}\right\}^{\mathrm{T}} \end{aligned} \tag{38}$$

where

$$\begin{aligned} &(-) = B, (+) = U, \beta = y, l = a, n = r \text{ if } \alpha = x \\ &(-) = L, (+) = R, \beta = x, l = b, n = s \text{ if } \alpha = y \end{aligned} \tag{39}$$

Using the method in Ref. [42], the Fourier series in exponential form is first rewritten as a trigonometric series. Then, by employing an orthogonal projection method, the spectral components satisfying the geometric and natural boundary conditions are separately extracted, so that the boundary functions and the general solution of the plate are matched under the same sine-cosine basis. In this way, the trigonometric series coefficients corresponding to each degree of freedom can be explicitly determined and associated with the corresponding external forces and deformations. In this process, the odd and even harmonics correspond to different constraint characteristics at the boundaries, ensuring that the boundary conditions are strictly satisfied numerically. Finally, by aligning the general solution with the spectral components of the boundary conditions through orthogonal integration, one obtains:

$$\begin{Bmatrix} \widetilde{\mathbf{d}}^{(\alpha)}_{n1} \\ \widetilde{\mathbf{f}}^{(\alpha)}_{n1} \end{Bmatrix} = \begin{cases} \dfrac{1}{\sqrt{\zeta_n l}}\displaystyle\int_{-l}^{l} \begin{Bmatrix} \mathbf{d}^{(\alpha)}_{o1}(\alpha) \\ \mathbf{f}^{(\alpha)}_{o1}(\alpha) \end{Bmatrix}\cos k_{\alpha n}\alpha \mathrm{d}\alpha & \text{if} \quad n = 0,2,4,\ldots,\dfrac{N_\alpha}{2} \\ \dfrac{1}{\sqrt{\zeta_n l}}\displaystyle\int_{-l}^{l} \begin{Bmatrix} \mathbf{d}^{(\alpha)}_{o1}(\alpha) \\ \mathbf{f}^{(\alpha)}_{o1}(\alpha) \end{Bmatrix}\sin k_{\alpha n}\alpha \mathrm{d}\alpha & \text{if} \quad n = 1,3,5,\ldots,\left(\dfrac{N_\alpha}{2}-1\right) \end{cases}$$
$$\begin{Bmatrix} \widetilde{\mathbf{d}}^{(\alpha)}_{n2} \\ \widetilde{\mathbf{f}}^{(\alpha)}_{n2} \end{Bmatrix} = \begin{cases} \dfrac{1}{\sqrt{\zeta_n l}}\displaystyle\int_{-l}^{l} \begin{Bmatrix} \mathbf{d}^{(\alpha)}_{o2}(\alpha) \\ \mathbf{f}^{(\alpha)}_{o2}(\alpha) \end{Bmatrix}\sin k_{\alpha n}\alpha \mathrm{d}\alpha & \text{if} \quad n = 2,4,6,\ldots,\dfrac{N_\alpha}{2} \\ \dfrac{1}{\sqrt{\zeta_n l}}\displaystyle\int_{-l}^{l} \begin{Bmatrix} \mathbf{d}^{(\alpha)}_{o2}(\alpha) \\ \mathbf{f}^{(\alpha)}_{o2}(\alpha) \end{Bmatrix}\cos k_{\alpha n}\alpha \mathrm{d}\alpha & \text{if} \quad n = 1,3,5,\ldots,\left(\dfrac{N_\alpha}{2}-1\right) \end{cases} \tag{40}$$

By substituting Eqs. (13) and (34) into Eq. (40), the following equations can be obtained:

$$\begin{aligned}\widetilde{\mathbf{d}}_{n1}^{(\alpha)} &= \begin{Bmatrix} \mathbf{h}_{n1(1)}^{(\alpha)} \\ \mathbf{h}_{n1(2)}^{(\alpha)} \end{Bmatrix} \left(n = 0, 1, 2, \ldots, \frac{N_\alpha}{2}\right) \\ \widetilde{\mathbf{d}}_{n2}^{(\alpha)} &= \mathbf{h}_{n2}^{(\alpha)}, \left(n = 1, 2, 3, \ldots, \frac{N_\alpha}{2}\right)\end{aligned} \tag{41}$$

$$\begin{aligned}\mathbf{h}_{n1(1)}^{(\alpha)} &= \widehat{o}_{n1}\mathbf{E}_{n1}^{(\alpha)}\overline{\mathbf{v}}_{n1}^{(\alpha)} + \sum_{\frac{N_\beta}{2}}^{m=0}\mathbf{\Phi}_{mn1}^{(\beta)}\overline{\mathbf{v}}_{m1}^{(\beta)} \\ \mathbf{h}_{n1(2)}^{(\alpha)} &= \widehat{o}_{n1}\left\{\mathbf{E}_{n1}^{(\alpha)}\mathbf{\Gamma}_{n1}^{\phi\beta(\alpha)}\overline{\mathbf{v}}_{n1}^{(\alpha)} + \mathbf{E}_{n2}^{(\alpha)}\mathbf{\Gamma}_{n2}^{\phi\beta(\alpha)}\overline{\mathbf{v}}_{n2}^{(\alpha)}\right\} \\ \mathbf{h}_{n2}^{(\alpha)} &= \widehat{o}_{n2}\left\{\mathbf{E}_{n1}^{(\alpha)}\mathbf{\Gamma}_{n1}^{\phi\alpha(\alpha)}\overline{\mathbf{v}}_{n1}^{(\alpha)} + \mathbf{E}_{n2}^{(\alpha)}\mathbf{\Gamma}_{n2}^{\phi\alpha(\alpha)}\overline{\mathbf{v}}_{n2}^{(\alpha)}\right\} \\ &+ \sum_{N_\beta/2}^{m=0}\Lambda_{mn1}^{(\beta)}\Gamma_{m1}^{\phi\alpha(\beta)}\widetilde{\mathbf{v}}_{m1}^{(\beta)} + \sum_{N_\beta/2}^{m=1}\Lambda_{mn2}^{(\beta)}\Gamma_{m2}^{\phi\alpha(\beta)}\widetilde{\mathbf{v}}_{m2}^{(\beta)}\end{aligned} \tag{42}$$

where

$$\begin{aligned}&\beta = y,\ n = r,\ m = q \text{ if } \alpha = x; \\ &\beta = x,\ n = s,\ m = p \text{ if } \alpha = y.\end{aligned} \tag{43}$$

The definition of the above functions can be found in Appendix B. Eq. (41) can be simplified to

$$\widetilde{\mathbf{d}} = \mathbf{H}(\omega)\overline{\mathbf{v}} \tag{44}$$

where $\mathbf{H}$ is a $3(N_x+N_y)+8 \times 3(N_x+N_y)+8$ matrix, and $\widetilde{\mathbf{d}}$ and $\overline{\mathbf{v}}$ are $3(N_x+N_y)+8 \times 1$ vectors, defined as:

$$\widetilde{\mathbf{d}} = \begin{Bmatrix} \widetilde{\mathbf{d}}_1^{(x)} \\ \widetilde{\mathbf{d}}_2^{(x)} \\ \widetilde{\mathbf{d}}_1^{(y)} \\ \widetilde{\mathbf{d}}_2^{(y)} \end{Bmatrix}, \overline{\mathbf{v}} = \begin{Bmatrix} \overline{\mathbf{v}}_1^{(x)} \\ \overline{\mathbf{v}}_2^{(x)} \\ \overline{\mathbf{v}}_1^{(y)} \\ \overline{\mathbf{v}}_2^{(y)} \end{Bmatrix} \tag{45}$$

where

$$\begin{aligned}\mathbf{d}_1^{(x)} &= \begin{Bmatrix} \mathbf{d}_{01}^{(x)} \\ \mathbf{d}_{11}^{(x)} \\ \mathbf{d}_{21}^{(x)} \\ \vdots \\ \mathbf{d}_{\left(\frac{N_x}{2}-1\right)1}^{(x)} \\ \mathbf{d}_{\left(\frac{N_x}{2}\right)1}^{(x)} \end{Bmatrix}, \mathbf{d}_1^{(y)} = \begin{Bmatrix} \mathbf{d}_{01}^{(y)} \\ \mathbf{d}_{11}^{(y)} \\ \mathbf{d}_{21}^{(y)} \\ \vdots \\ \mathbf{d}_{\left(\frac{N_y}{2}-1\right)1}^{(y)} \\ \mathbf{d}_{\left(\frac{N_y}{2}\right)1}^{(y)} \end{Bmatrix}, \mathbf{d}_2^{(x)} = \begin{Bmatrix} \mathbf{d}_{12}^{(x)} \\ \mathbf{d}_{22}^{(x)} \\ \mathbf{d}_{32}^{(x)} \\ \vdots \\ \mathbf{d}_{\left(\frac{N_x}{2}-1\right)2}^{(x)} \\ \mathbf{d}_{\left(\frac{N_x}{2}\right)2}^{(x)} \end{Bmatrix}, \mathbf{d}_2^{(y)} \\ &= \begin{Bmatrix} \mathbf{d}_{12}^{(y)} \\ \mathbf{d}_{22}^{(y)} \\ \mathbf{d}_{32}^{(y)} \\ \vdots \\ \mathbf{d}_{\left(\frac{N_y}{2}-1\right)2}^{(y)} \\ \mathbf{d}_{\left(\frac{N_y}{2}\right)2}^{(y)} \end{Bmatrix}\end{aligned} \tag{46}$$

$$\begin{aligned}\overline{\mathbf{v}}_1^{(x)} &= \begin{Bmatrix} \overline{\mathbf{v}}_{01}^{(x)} \\ \overline{\mathbf{v}}_{11}^{(x)} \\ \overline{\mathbf{v}}_{21}^{(x)} \\ \vdots \\ \overline{\mathbf{v}}_{\left(\frac{N_x}{2}-1\right)1}^{(x)} \\ \overline{\mathbf{v}}_{\left(\frac{N_x}{2}\right)1}^{(x)} \end{Bmatrix}, \overline{\mathbf{v}}_1^{(y)} = \begin{Bmatrix} \overline{\mathbf{v}}_{01}^{(y)} \\ \overline{\mathbf{v}}_{11}^{(y)} \\ \overline{\mathbf{v}}_{21}^{(y)} \\ \vdots \\ \overline{\mathbf{v}}_{\left(\frac{N_y}{2}-1\right)1}^{(y)} \\ \overline{\mathbf{v}}_{\left(\frac{N_y}{2}\right)1}^{(y)} \end{Bmatrix}, \overline{\mathbf{v}}_2^{(x)} = \begin{Bmatrix} \overline{\mathbf{v}}_{12}^{(x)} \\ \overline{\mathbf{v}}_{22}^{(x)} \\ \overline{\mathbf{v}}_{32}^{(x)} \\ \vdots \\ \overline{\mathbf{v}}_{\left(\frac{N_x}{2}-1\right)2}^{(x)} \\ \overline{\mathbf{v}}_{\left(\frac{N_x}{2}\right)2}^{(x)} \end{Bmatrix}, \overline{\mathbf{v}}_2^{(y)} \\ &= \begin{Bmatrix} \overline{\mathbf{v}}_{12}^{(y)} \\ \overline{\mathbf{v}}_{22}^{(y)} \\ \overline{\mathbf{v}}_{32}^{(y)} \\ \vdots \\ \overline{\mathbf{v}}_{\left(\frac{N_y}{2}-1\right)2} \\ \overline{\mathbf{v}}_{\left(\frac{N_y}{2}\right)2}^{(y)} \end{Bmatrix}.\end{aligned} \tag{47}$$

Substituting Eqs. (13) and (34) into Eqs. (3), (4), and (5), and substituting the results into Eq. (2) and further into Eq. (40), the following functions are obtained:

$$\begin{aligned}\widetilde{\mathbf{f}}_{n1}^{(x)} &= \begin{Bmatrix} \mathbf{g}_{n1(1)}^{(x)} \\ \mathbf{g}_{n1(2)}^{(x)} \end{Bmatrix}, \left(n = 0, 1, 2, \ldots, \frac{N_x}{2}\right) \\ \widetilde{\mathbf{f}}_{n2}^{(x)} &= \mathbf{g}_{n2}^{(x)}, \left(n = 1, 2, 3, \ldots, \frac{N_x}{2}\right)\end{aligned} \tag{48}$$

$$\begin{aligned}\widetilde{\mathbf{f}}_{n1}^{(y)} &= \begin{Bmatrix} \mathbf{g}_{n1(1)}^{(y)} \\ \mathbf{g}_{n1(2)}^{(y)} \end{Bmatrix}, \left(n = 0, 1, 2, \ldots, \frac{N_y}{2}\right) \\ \widetilde{\mathbf{f}}_{n2}^{(y)} &= \mathbf{g}_{n2}^{(x)}, \left(n = 1, 2, 3, \ldots, \frac{N_y}{2}\right)\end{aligned} \tag{49}$$

where

$$\begin{aligned}\mathbf{g}_{n1(1)}^{(x)} &= -C_{55}\widehat{o}_{n1}\mathbf{I}\left\{\mathbf{E}_{n1}^{(x)}\left[\chi_{n1}^{(x)} - \mathbf{\Gamma}_{n1}^{\phi y(x)}\right]\overline{\mathbf{v}}_{n1}^{(x)} - \mathbf{E}_{n2}^{(x)}\mathbf{\Gamma}_{n2}^{\phi y(x)}\overline{\mathbf{v}}_{n2}^{(x)}\right\} \\ \mathbf{g}_{n1(2)}^{(x)} &= -\widehat{o}_{n1}\mathbf{I}\mathbf{E}_{n1}^{(x)}\left[D_{11}\mathbf{\Gamma}_{n1}^{\phi y(x)}\chi_{n1}^{(x)} + D_{12}\mathbf{\Gamma}_{n1}^{\phi x(x)}\xi_{n1}^{(x)}\right]\overline{\mathbf{v}}_{n1}^{(x)} \\ &-\widehat{o}_{n1}\mathbf{I}\mathbf{E}_{n2}^{(x)}\left[D_{11}\mathbf{\Gamma}_{n2}^{\phi y(x)}\chi_{n2}^{(x)} + D_{12}\mathbf{\Gamma}_{n2}^{\phi x(x)}\xi_{n2}^{(x)}\right]\overline{\mathbf{v}}_{n2}^{(x)} \\ &-\mathbf{I}\sum_{m=0}^{\frac{N_x}{2}-1}\mathbf{\Phi}_{mn1}^{(y)}\left[D_{11}\mathbf{\Gamma}_{m1}^{\phi y(y)}\xi_{m1}^{(y)} + D_{12}\mathbf{\Gamma}_{m1}^{\phi x(y)}\chi_{m1}^{(y)}\right]\overline{\mathbf{v}}_{m1}^{(y)} \\ &-\mathbf{I}\sum_{m=1}^{2}\mathbf{\Phi}_{mn2}^{(y)}\left[D_{11}\mathbf{\Gamma}_{m2}^{\phi y(y)}\xi_{m2}^{(y)} + D_{12}\mathbf{\Gamma}_{m2}^{\phi x(y)}\chi_{m2}^{(y)}\right]\overline{\mathbf{v}}_{m2}^{(y)} \\ \mathbf{g}_{n2}^{(x)} &= D_{66}\widehat{o}_{n2}\mathbf{I}\mathbf{E}_{n1}^{(x)}\left[\mathbf{\Gamma}_{n1}^{\phi y(x)}\xi_{n1}^{(x)} + \mathbf{\Gamma}_{n1}^{\phi x(x)}\chi_{n1}^{(x)}\right]\overline{\mathbf{v}}_{n1}^{(x)} \\ &+D_{66}\widehat{o}_{n2}\mathbf{I}\mathbf{E}_{n2}^{(x)}\left[\mathbf{\Gamma}_{n2}^{\phi y(x)}\xi_{n2}^{(x)} + \mathbf{\Gamma}_{n2}^{\phi x(x)}\chi_{n2}^{(x)}\right]\overline{\mathbf{v}}_{n2}^{(x)}\end{aligned} \tag{50}$$

$$\mathbf{g}_{n1(1)}^{(y)} = -C_{44}\widehat{o}_{n1}\mathbf{I}\left\{\mathbf{E}_{n1}^{(y)}\left[\chi_{n1}^{(y)} - \mathbf{\Gamma}_{n1}^{\phi x(y)}\right]\overline{\mathbf{v}}_{n1}^{(y)} - \mathbf{E}_{n2}^{(y)}\mathbf{\Gamma}_{n2}^{\phi x(y)}\overline{\mathbf{v}}_{n2}^{(y)}\right\}$$

$$\begin{aligned}
\mathbf{g}_{n1(2)}^{(y)} = & -\widehat{o}_{n1}\mathbf{I}\mathbf{E}_{n1}^{(y)}\left[D_{22}\mathbf{\Gamma}_{n1}^{\phi x(y)}\chi_{n1}^{(y)} + D_{21}\mathbf{\Gamma}_{n1}^{\phi y(y)}\xi_{n1}^{(y)}\right]\overline{\mathbf{v}}_{n1}^{(x)} \\
& -\widehat{o}_{n1}\mathbf{I}\mathbf{E}_{n2}^{(y)}\left[D_{22}\mathbf{\Gamma}_{n2}^{\phi x(y)}\chi_{n2}^{(y)} + D_{21}\mathbf{\Gamma}_{n2}^{\phi y(y)}\xi_{n2}^{(y)}\right]\overline{\mathbf{v}}_{n2}^{(y)} \\
& -\mathbf{I}\sum_{m=0}^{\frac{N_y}{2}-1}\mathbf{\Phi}_{mn1}^{(x)}\left[D_{22}\mathbf{\Gamma}_{m1}^{\phi x(x)}\xi_{m1}^{(x)} + D_{21}\mathbf{\Gamma}_{m1}^{\phi y(x)}\chi_{m1}^{(x)}\right]\overline{\mathbf{v}}_{m1}^{(x)} \\
& -\mathbf{I}\sum_{m=1}^{\frac{N_x}{2}-1}\mathbf{\Phi}_{mn2}^{(x)}\left[D_{22}\mathbf{\Gamma}_{m2}^{\phi x(x)}\xi_{m2}^{(x)} + D_{21}\mathbf{\Gamma}_{m2}^{\phi y(x)}\chi_{m2}^{(x)}\right]\overline{\mathbf{v}}_{m2}^{(x)} \\
\mathbf{g}_{n2}^{(y)} = & D_{66}\widehat{o}_{n2}\mathbf{I}\mathbf{E}_{n1}^{(y)}\left[\mathbf{\Gamma}_{n1}^{\phi x(y)}\xi_{n1}^{(y)} + \mathbf{\Gamma}_{n1}^{\phi y(y)}\chi_{n1}^{(y)}\right]\overline{\mathbf{v}}_{n1}^{(y)} \\
& + D_{66}\widehat{o}_{n2}\mathbf{I}\mathbf{E}_{n2}^{(y)}\left[\mathbf{\Gamma}_{n2}^{\phi x(y)}\xi_{n2}^{(y)} + \mathbf{\Gamma}_{n2}^{\phi y(y)}\chi_{n2}^{(y)}\right]\overline{\mathbf{v}}_{n2}^{(y)}
\end{aligned} \tag{51}$$

The definition of the functions in Eqs. (50) and (51) can be found in Appendix B.

Eqs. (48) and (49) can be simplified as

$$\widetilde{\mathbf{f}} = \mathbf{G}(\omega)\overline{\mathbf{v}} \tag{52}$$

where $\mathbf{G}$ denotes a $3(N_x+N_y)+8 \times 3(N_x+N_y)+8$ matrix, $\widetilde{\mathbf{f}}$ denoted a $3(N_x+N_y)+8 \times 1$ vector, which is defined as:

$$\widetilde{\mathbf{f}} = \begin{Bmatrix} \widetilde{\mathbf{f}}_1^{(x)} \\ \widetilde{\mathbf{f}}_2^{(x)} \\ \widetilde{\mathbf{f}}_1^{(y)} \\ \widetilde{\mathbf{f}}_2^{(y)} \end{Bmatrix} \tag{53}$$

where

$$\mathbf{f}_1^{(x)} = \begin{Bmatrix} \mathbf{f}_{01}^{(x)} \\ \mathbf{f}_{11}^{(x)} \\ \mathbf{f}_{21}^{(x)} \\ \vdots \\ \mathbf{f}_{\left(\frac{N_x}{2}-1\right)1}^{(x)} \\ \mathbf{f}_{\left(\frac{N_x}{2}\right)1}^{(x)} \end{Bmatrix}, \mathbf{f}_1^{(y)} = \begin{Bmatrix} \mathbf{f}_{01}^{(y)} \\ \mathbf{f}_{11}^{(y)} \\ \mathbf{f}_{21}^{(y)} \\ \vdots \\ \mathbf{f}_{\left(\frac{N_y}{2}-1\right)1}^{(y)} \\ \mathbf{f}_{\left(\frac{N_y}{2}\right)1}^{(y)} \end{Bmatrix}, \mathbf{f}_2^{(x)} = \begin{Bmatrix} \mathbf{f}_{12}^{(x)} \\ \mathbf{f}_{22}^{(x)} \\ \mathbf{f}_{32}^{(x)} \\ \vdots \\ \mathbf{f}_{\left(\frac{N_x}{2}-1\right)2}^{(x)} \\ \mathbf{f}_{\left(\frac{N_x}{2}\right)2}^{(x)} \end{Bmatrix}, \mathbf{f}_2^{(y)} = \begin{Bmatrix} \mathbf{f}_{12}^{(y)} \\ \mathbf{f}_{22}^{(y)} \\ \mathbf{f}_{32}^{(y)} \\ \vdots \\ \mathbf{f}_{\left(\frac{N_y}{2}-1\right)2}^{(y)} \\ \mathbf{f}_{\left(\frac{N_y}{2}\right)2}^{(y)} \end{Bmatrix} \tag{54}$$

By simultaneously solving Eqs. (44) and (52) and eliminating $\overline{\mathbf{v}}$, the relation between force and displacement can be obtained as:

$$\mathbf{S}(\omega)\widetilde{\mathbf{d}} = \widetilde{\mathbf{f}} \tag{55}$$

where $\mathbf{S}(\omega)$ is the spectral element matrix, defined as:

$$\mathbf{S}(\omega) = \mathbf{G}\mathbf{H}^{-1} \tag{56}$$

Table 1
The first ten natural frequencies obtained using SEM, from the results in Ref. [42] and FEM ($E = 69$ GPa, $2a = 2b = 1$ m, $h = 0.1$ m, $\rho = 2700$ kg/m^3, $\nu = 0.3$, $\kappa = 5/6$).

Modes	SEM (Hz) N_x=N_y=2^7[42]	FEM (Hz) 200 × 200 Elements	SEM (Hz) N_x=N_y=2^5	SEM (Hz) N_x=N_y=2^7
1	309.7	309.69	309.48	309.68
2	461.2	461.45	461.20	461.17
3	567.9	568.03	567.25	567.86
4	777.2	777.25	777.24	777.21
5	1348	1348.55	1348.07	1348.06
6	1356	1357.13	1356.21	1356.13
7	1476	1476.46	1477.06	1476.42
8	1648	1648.34	1647.93	1648.26
9	2135	2135.85	2134.36	2134.82
10	2395	2396.94	2395.67	2395.36

2.5. Free vibration analysis

After obtaining the spectral element matrix $\mathbf{S}(\omega)$ of the orthotropic Mindlin plate, the condition $\det(\mathbf{S}(\omega))=0$ can be set to determine the plate's natural frequencies ω_i, where i is the mode number. Subsequently, substituting ω_i into $\mathbf{S}(\omega)\widetilde{\mathbf{d}} = 0$ to calculate $\widetilde{\mathbf{d}}$, and then obtaining the spectral components $\overline{\mathbf{v}}$ of the general solution through Eq. (44). At this point, $\overline{\mathbf{v}}$ represents the spectral components for $p = 0 \sim N_x/2$ and $q = 0 \sim N_y/2$, and the complete spectral components $\overline{\mathbf{v}}$ ($p = -N_x/2 \sim (N_x/2) - 1$ and $q = -N_y/2 \sim (N_y/2) - 1$) can be obtained using Eq. (30). By substituting the complete spectral components$\overline{v}$into Eq. (34), the i^{th} mode shape shall be determined. The spectral element matrix $\mathbf{S}(\omega)$ of each unit can be assembled into the global spectral element matrix $\mathbf{S}_g(\omega)$ in the identical manner to the assembly of the global stiffness matrix in FEM.

3. Numerical examples

This section explores the feasibility of the spectral element model for orthotropic Mindlin plates using numerical methods. First, the spectral element model is employed to calculate the first ten natural frequencies of isotropic Mindlin plates and compare them with the results [42] to affirm the model's convergence and accuracy. The first six mode shapes are plotted. The results of this study are also compared with the DSM and FEM calculations for orthotropic Mindlin plates presented in Ref. [35] to confirm the applicability of the spectral element model in solving orthotropic plates. Finally, the natural frequencies of orthotropic Mindlin plates under CFCF (Clamped-Free-Clamped-Free), FFFF (Free--Free-Free-Free), SSSS (all edges are simply supported) and CSFS (Clamped-Supported-Free-Supported) boundary conditions are computed, and the first six mode shapes are illustrated for the FFFF and CSFS boundary conditions as example.

In Table 1, a comparison is presented of the first ten natural frequencies of isotropic square plates under FFFF boundary conditions. These frequencies were calculated using the spectral element model that was proposed, from the results in Ref. [42], and FEM. In this study, the spectral element model was tested with sampling numbers of 2^5 and 2^7 to evaluate its accuracy and convergence. As shown in the table, when the sampling number is set to 2^5, the results obtained through calculation agree well with those in Ref. [42]. When the sampling number is increased to 2^7, the results perfectly match those in Ref. [42]. Fig. 2 displays the mode shapes to the first six natural frequencies obtained using the spectral element model.

After verifying the applicability of the spectral element model in isotropic plate problems, the first ten natural frequencies of a square orthotropic glass/epoxy Mindlin plate (with material properties $E_{xy} = 60.7$ GPa, $E_{yx} = 24.8$ GPa, $a/b = 1$, $h/a = 0.1$, $\nu_{xy} = 0.23$, $\kappa = 0.8601$, $G_{xy} = G_{xz} = G_{yz} = 12$ GPa) were further computed. Table 2 compares the first ten Non-dimensional natural frequencies $\left(\Omega_n = a\sqrt[4]{\omega^2\rho h/D_{11}}\right)$ obtained

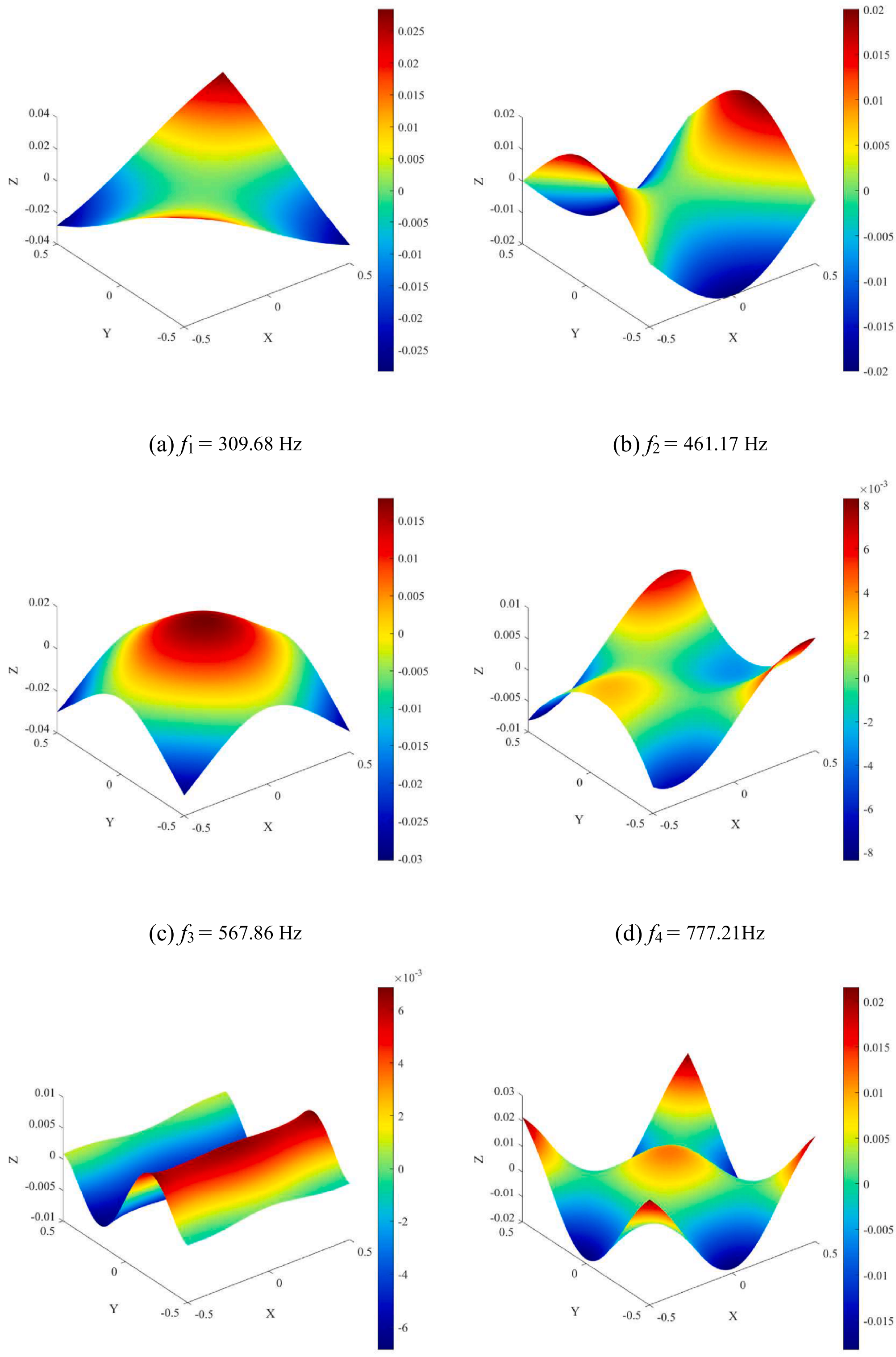

(a) $f_1 = 309.68$ Hz (b) $f_2 = 461.17$ Hz

(c) $f_3 = 567.86$ Hz (d) $f_4 = 777.21$Hz

(e) $f_5 = 1348.06$Hz (f) $f_6 = 1356.13$Hz

Fig. 2. The first six natural frequencies and their corresponding mode shapes for an isotropic square plate under FFFF boundary conditions.

using SEM, the DSM [35], and FEM. The results show that the SEM results are within a 0.6 % error compared to both DSM and FEM, demonstrating the feasibility of the spectral element model in analyzing orthotropic Mindlin plates.

After verifying that the spectral element model can be effectively applied to the solution of orthotropic plates, the natural frequencies of a graphite/epoxy orthotropic Mindlin plate (with material properties $E_{xy} = 185$ GPa, $E_{yx} = 10.5$ GPa, $a = b = 1$ m, $h/a = 0.1$, $\nu_{xy} = 0.28$, $\kappa = 5/6$,

Table 2
The first ten non-dimensional natural frequencies (Hz) of a square glass/epoxy plate under FFFF boundary conditions.

Modes	DSM [35]	FEM 200 × 200 Elements	SEM					
			N_x=N_y=2^5	Err1(%)	Err2(%)	N_x=N_y=2^7	Err1(%)	Err2(%)
1	1.5643	1.5606	1.5601	0.27	0.03	1.5596	0.30	0.06
2	1.8716	1.8583	1.8636	0.43	0.29	1.8618	0.52	0.19
3	2.3503	2.3423	2.3468	0.15	0.19	2.3466	0.16	0.18
4	2.4490	2.4407	2.4411	0.32	0.02	2.4380	0.45	0.11
5	2.6963	2.6810	2.6874	0.33	0.24	2.6885	0.29	0.28
6	3.1036	3.0816	3.0885	0.49	0.22	3.0852	0.59	0.12
7	3.4095	3.3993	3.3964	0.38	0.09	3.3935	0.47	0.17
8	3.4451	3.4307	3.4329	0.35	0.06	3.4254	0.57	0.15
9	3.8464	3.8171	3.8294	0.44	0.32	3.8292	0.45	0.32
10	4.0427	4.0252	4.0266	0.40	0.03	4.0266	0.40	0.03

Note: Err1 and Err2 represent the relative errors of the SEM calculations with respect to the DSM and FEM calculations, respectively.

Table 3
The first ten natural frequencies (Hz) of a square graphite/epoxy plate under CFCF boundary conditions.

Modes	FEM 200 × 200 Elements	SEM(Hz)			
		N_x=N_y=2^5	Err(%)	N_x=N_y=2^7	Err(%)
1	65.44	65.35	0.14	65.35	0.14
2	86.78	86.59	0.22	86.59	0.22
3	177.95	177.89	0.03	177.89	0.03
4	208.41	208.26	0.07	208.13	0.13
5	294.55	294.28	0.09	294.21	0.12
6	342.72	342.85	0.04	342.68	0.01
7	375.92	375.61	0.08	375.37	0.15
8	382.65	381.97	0.18	381.83	0.21
9	528.02	527.17	0.16	527.12	0.17
10	554.35	553.58	0.14	553.47	0.16

Note: Err represents the relative errors of the SEM calculations with FEM calculations.

Table 4
The first ten natural frequencies (Hz) of a square graphite/epoxy plate under FFFF boundary conditions.

Modes	FEM 200 × 200 Elements	SEM			
		N_x=N_y=2^5	Err(%)	N_x=N_y=2^7	Err(%)
1	54.81	54.76	0.09	54.75	0.11
2	65.32	64.79	0.81	64.46	1.31
3	127.60	127.08	0.41	127.13	0.37
4	178.09	176.26	1.03	176.81	0.72
5	238.97	242.45	1.46	240.48	0.63
6	265.04	265.44	0.15	265.44	0.15
7	284.94	281.87	1.08	281.85	1.08
8	345.08	345.59	0.15	344.17	0.26
9	389.20	389.45	0.06	389.59	0.10
10	446.74	446.42	0.07	446.57	0.04

Note: Err represents the relative errors of the SEM calculations with FEM calculations.

Table 5
The first ten natural frequencies (Hz) of a square graphite/epoxy plate under SSSS boundary conditions.

Modes	FEM 200 × 200 Elements	SEM			
		N_x=N_y=2^5	Err(%)	N_x=N_y=2^7	Err(%)
1	256.60	255.62	0.38	256.23	0.14
2	317.79	316.29	0.47	315.85	0.61
3	445.17	446.41	0.28	445.41	0.05
4	599.46	596.97	0.42	598.03	0.24
5	634.55	631.64	0.46	632.60	0.31
6	727.62	724.14	0.48	725.46	0.30
7	872.57	873.21	0.07	872.11	0.05
8	1028.20	1025.97	0.22	1025.91	0.22
9	1059.74	1062.77	0.29	1055.80	0.37
10	1074.56	1077.43	0.27	1072.94	0.15

Note: Err represents the relative errors of the SEM calculations with FEM calculations.

Table 6
The first ten natural frequencies (Hz) of a square graphite/epoxy plate under CSFS boundary conditions.

Modes	FEM 200 × 200 Elements	SEM			
		N_x=N_y=2^5	Err(%)	N_x=N_y=2^7	Err(%)
1	85.24	85.08	0.19	85.18	0.07
2	193.48	193.94	0.24	193.26	0.11
3	270.57	269.87	0.26	270.14	0.16
4	347.48	347.62	0.04	347.06	0.12
5	356.31	356.4	0.03	355.82	0.14
6	484.58	484.28	0.06	483.88	0.14
7	566.82	567.49	0.12	565.25	0.28
8	638.39	638.71	0.05	637.32	0.17
9	675.96	675.42	0.08	675.72	0.04
10	689.71	690.26	0.08	688.91	0.12

Note: Err represents the relative errors of the SEM calculations with FEM calculations.

$G_{xy} = G_{xz} = G_{yz} = 7.3$ GPa, $\rho = 1600$ kg/m^3) were further computed. Tables 3, 4, 5 **and** 6 present the calculation results under CFCF, FFFF, SSSS and CFSF boundary conditions, respectively. In all tables, the second column contains the results obtained by FEM with a discretization of 200 × 200 elements, while the third and fifth columns, respectively, present the results of SEM with 2^5 and 2^7 sampling points. The results show that the calculation errors of natural frequencies between SEM and FEM are within 1.5 %. Fig.3 and Fig.4 present the mode shapes of the first six natural frequencies obtained using SEM for FFFF and CSFS boundary conditions, respectively.

4. Conclusions

In referring to the spectral element modeling method proposed by Kim and Lee, this study proposes a spectral element model for orthotropic rectangular Mindlin plates with arbitrary boundary conditions, and its specific application methods in free vibration analysis are described. The accuracy and reliability of the proposed method for orthotropic rectangular Mindlin plates is demonstrated through a comparison with existing solutions, including SEM for isotropic plates, DSM for orthotropic plates, and the FEM for both types of plates. The spectral element model in this study can also be applied to the solution of dynamic response and wave propagation analysis in further study, as described in Ref. [42].

CRediT authorship contribution statement

Yunlai Zhou: Writing – original draft, Funding acquisition, Formal

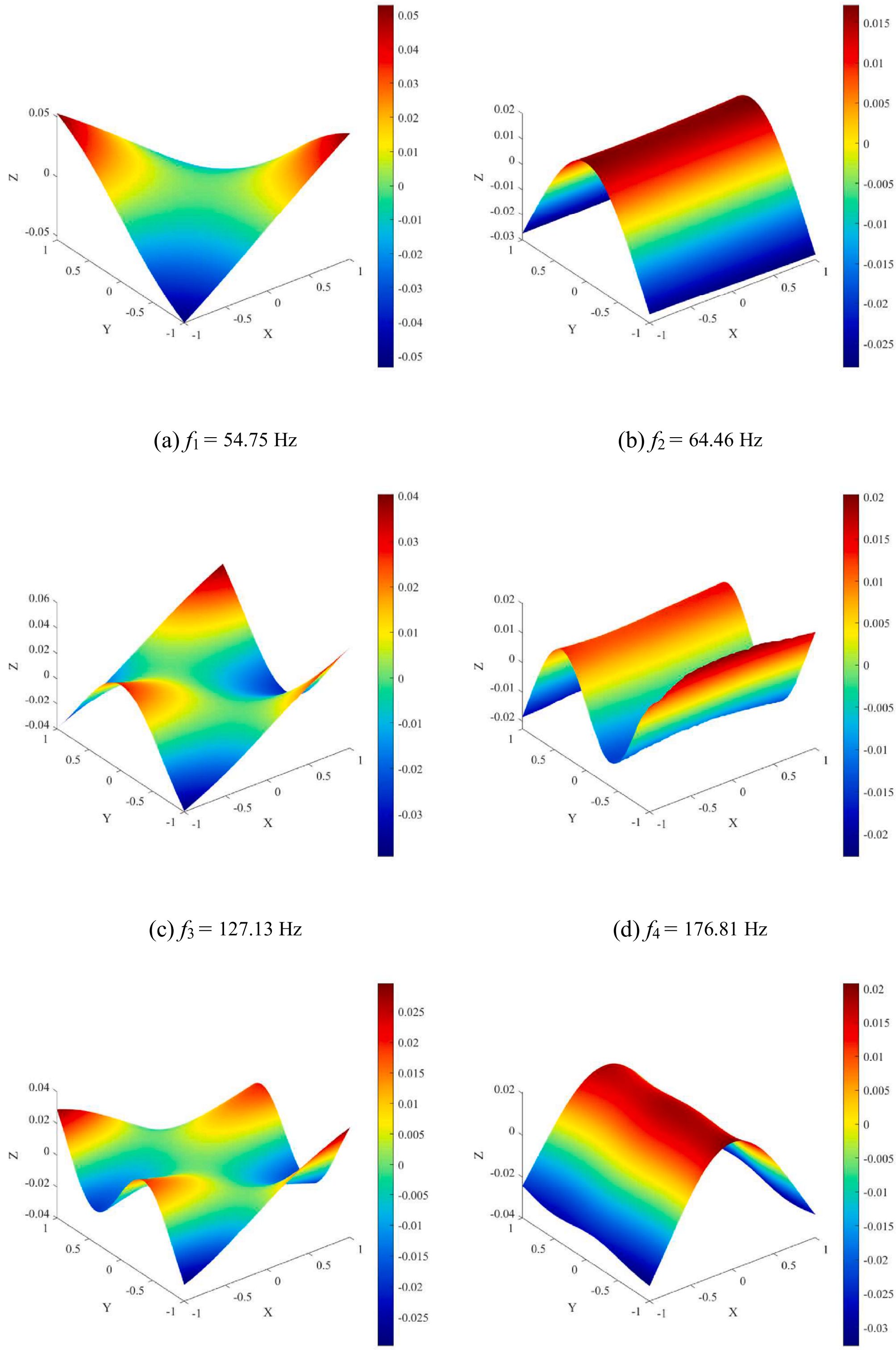

(a) $f_1 = 54.75$ Hz (b) $f_2 = 64.46$ Hz

(c) $f_3 = 127.13$ Hz (d) $f_4 = 176.81$ Hz

(e) $f_5 = 240.48$ Hz (f) $f_6 = 265.44$ Hz

Fig. 3. The mode shapes to the first six natural frequencies of a square graphite/epoxy plate under FFFF boundary conditions.

analysis, Methodology. **Feng Yao:** Methodology, Conceptualization. **Yubo Wang:** Conceptualization, Validation. **Chunyu Bai:** Formal analysis. **Shijie Liu:** Writing – review & editing. **Magd Abdel Wahab:** Writing – review & editing, Supervision.

Declaration of competing interest

The authors declare that they have no known competing financial interests or personal relationships that could have appeared to influence

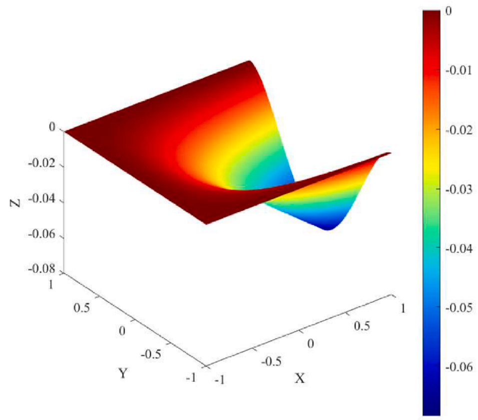

(a) $f_1 = 85.18$ Hz

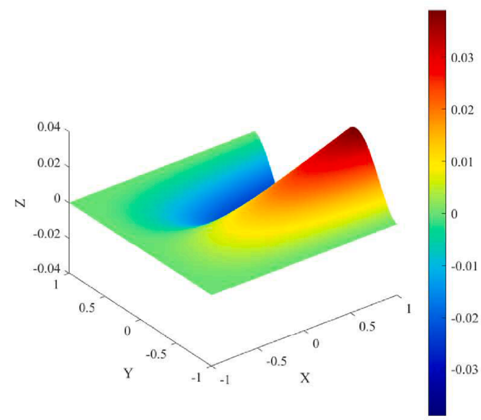

(b) $f_2 = 193.26$ Hz

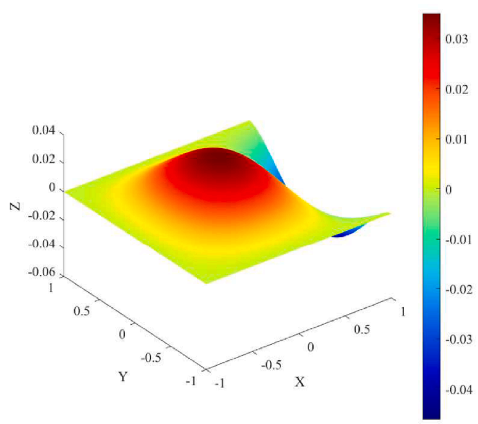

(c) $f_3 = 270.14$ Hz

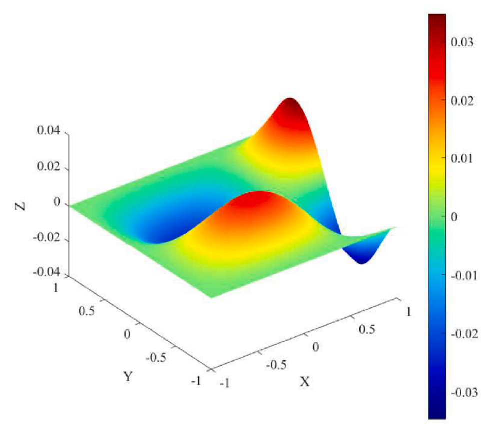

(d) $f_4 = 347.06$ Hz

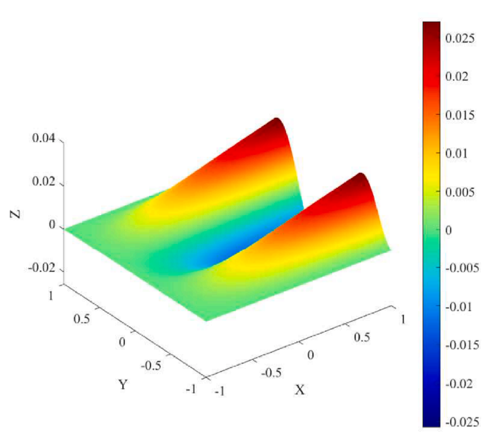

(e) $f_5 = 355.82$ Hz

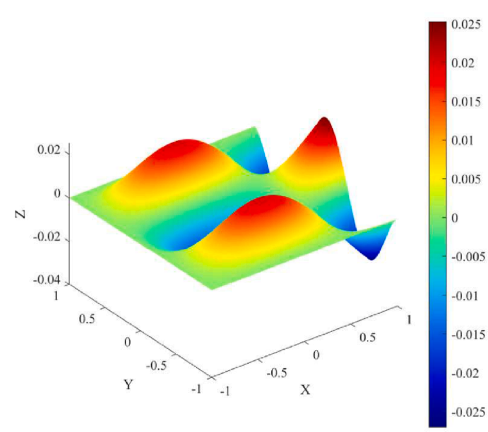

(f) $f_6 = 483.88$ Hz

Fig. 4. The mode shapes to the first six natural frequencies of a square graphite/epoxy plate under CSFS boundary conditions.

the work reported in this paper.

Acknowledgement

The authors acknowledge the support of Youth Top Talent Program of Xi'an Jiaotong University.

Appendix A

The definition of the functions in Eq. (26) is as follows:

$$
\begin{aligned}
\mathbf{z}_p^{(x)}(y) &= \frac{1}{\sqrt{\zeta_p a}}\begin{bmatrix} \mathbf{e}_{p1}^{(x)}(y) & 0_{1\times 2} \\ \mathbf{e}_{p1}^{(x)}(y)\boldsymbol{\Gamma}_{p1}^{\phi x(x)} & 0_{1\times 2} \\ \mathbf{e}_{p1}^{(x)}(y)\boldsymbol{\Gamma}_{p1}^{\phi y(x)} & 0_{1\times 2} \\ 0_{1\times 4} & \mathbf{e}_{p2}^{(x)}(y)\boldsymbol{\Gamma}_{p2}^{\phi x(x)} \\ 0_{1\times 4} & \mathbf{e}_{p2}^{(x)}(y)\boldsymbol{\Gamma}_{p2}^{\phi y(x)} \end{bmatrix} \\
\mathbf{z}_q^{(y)}(x) &= \frac{1}{\sqrt{\zeta_q b}}\begin{bmatrix} \mathbf{e}_{q1}^{(y)}(x) & 0_{1\times 2} \\ \mathbf{e}_{q1}^{(y)}(x)\boldsymbol{\Gamma}_{q1}^{\phi x(y)} & 0_{1\times 2} \\ \mathbf{e}_{q1}^{(y)}(x)\boldsymbol{\Gamma}_{q1}^{\phi y(y)} & 0_{1\times 2} \\ 0_{1\times 4} & \mathbf{e}_{q2}^{(y)}(x)\boldsymbol{\Gamma}_{q2}^{\phi x(y)} \\ 0_{1\times 4} & \mathbf{e}_{q2}^{(y)}(x)\boldsymbol{\Gamma}_{q2}^{\phi y(y)} \end{bmatrix}
\end{aligned}
\tag{A.1}
$$

$$
\begin{aligned}
\widehat{\mathbf{v}}_{p1}^{(x)} &= \left\{ v_{p1(1)}^{(x)}, v_{p1(2)}^{(x)}, v_{p1(3)}^{(x)}, v_{p1(4)}^{(x)} \right\}^{\mathrm{T}} \\
\widehat{\mathbf{v}}_{p2}^{(x)} &= \left\{ v_{p1(5)}^{(x)}, v_{p1(6)}^{(x)} \right\}^{\mathrm{T}} \\
\widehat{\mathbf{v}}_{q1}^{(x)} &= \left\{ v_{q1(1)}^{(y)}, v_{q1(2)}^{(y)}, v_{q1(3)}^{(y)}, v_{q1(4)}^{(y)} \right\}^{\mathrm{T}} \\
\widehat{\mathbf{v}}_{q2}^{(x)} &= \left\{ v_{q1(5)}^{(x)}, v_{q1(6)}^{(x)} \right\}^{\mathrm{T}}
\end{aligned}
\tag{A.2}
$$

where $0_{m\times n}$ represents the zero matrix of $m \times n$.

$$
\zeta_p = \begin{cases} 2 & \text{if } p = 0 \\ 1 & \text{if } p \neq 0 \end{cases}, \zeta_q = \begin{cases} 2 & \text{if } q = 0 \\ 1 & \text{if } q \neq 0 \end{cases}
\tag{A.3}
$$

$$
\begin{aligned}
\mathbf{e}_{p1}^{(x)}(y) &= \begin{Bmatrix} \mathrm{e}^{\mathrm{i}K_{xp(1)}y - \mathrm{i}\hat{K}_{xp(1)}b} \\ \mathrm{e}^{\mathrm{i}K_{xp(2)}y - \mathrm{i}\hat{K}_{xp(2)}b} \\ \mathrm{e}^{\mathrm{i}K_{xp(3)}y - \mathrm{i}\hat{K}_{xp(3)}b} \\ \mathrm{e}^{\mathrm{i}K_{xp(4)}y - \mathrm{i}\hat{K}_{xp(4)}b} \end{Bmatrix}^{\mathrm{T}}, \quad \mathbf{e}_{q1}^{(y)}(x) = \begin{Bmatrix} \mathrm{e}^{\mathrm{i}K_{yq(1)}x - \mathrm{i}\hat{K}_{yq(1)}a} \\ \mathrm{e}^{\mathrm{i}K_{yq(2)}x - \mathrm{i}\hat{K}_{yq(2)}a} \\ \mathrm{e}^{\mathrm{i}K_{yq(3)}x - \mathrm{i}\hat{K}_{yq(3)}a} \\ \mathrm{e}^{\mathrm{i}K_{yq(4)}x - \mathrm{i}\hat{K}_{yq(4)}a} \end{Bmatrix}^{\mathrm{T}} \\
\mathbf{e}_{p2}^{(x)}(y) &= \begin{Bmatrix} \mathrm{e}^{\mathrm{i}K_{xp(5)}y - \mathrm{i}\hat{K}_{xp(5)}b} \\ \mathrm{e}^{\mathrm{i}K_{xp(6)}y - \mathrm{i}\hat{K}_{xp(6)}b} \end{Bmatrix}^{\mathrm{T}}, \quad \mathbf{e}_{q2}^{(y)}(y) = \begin{Bmatrix} \mathrm{e}^{\mathrm{i}K_{yq(5)}x - \mathrm{i}\hat{K}_{yq(5)}a} \\ \mathrm{e}^{\mathrm{i}K_{yq(6)}y - \mathrm{i}\hat{K}_{yq(6)}a} \end{Bmatrix}^{\mathrm{T}}
\end{aligned}
\tag{A.4}
$$

$$\begin{aligned}
\boldsymbol{\Gamma}_{p1}^{\phi x(x)} &= \mathrm{diag}\left[\frac{v_{p2(1)}^{(x)}}{v_{p1(1)}^{(x)}},\frac{v_{p2(2)}^{(x)}}{v_{p1(2)}^{(x)}},\frac{v_{p2(3)}^{(x)}}{v_{p1(3)}^{(x)}},\frac{v_{p2(4)}^{(x)}}{v_{p1(4)}^{(x)}}\right]\\
\boldsymbol{\Gamma}_{p1}^{\phi y(x)} &= \mathrm{diag}\left[\frac{v_{p3(1)}^{(x)}}{v_{p1(1)}^{(x)}},\frac{v_{p3(2)}^{(x)}}{v_{p1(2)}^{(x)}},\frac{v_{p3(3)}^{(x)}}{v_{p1(3)}^{(x)}},\frac{v_{p3(4)}^{(x)}}{v_{p1(4)}^{(x)}}\right]\\
\boldsymbol{\Gamma}_{q1}^{\phi x(y)} &= \mathrm{diag}\left[\frac{v_{q2(1)}^{(y)}}{v_{q1(1)}^{(y)}},\frac{v_{q2(2)}^{(y)}}{v_{q1(2)}^{(y)}},\frac{v_{q2(3)}^{(y)}}{v_{q1(3)}^{(y)}},\frac{v_{q2(4)}^{(y)}}{v_{q1(4)}^{(y)}}\right]\\
\boldsymbol{\Gamma}_{q1}^{\phi y(y)} &= \mathrm{diag}\left[\frac{v_{q3(1)}^{(y)}}{v_{q1(1)}^{(y)}},\frac{v_{q3(2)}^{(y)}}{v_{q1(2)}^{(y)}},\frac{v_{q3(3)}^{(y)}}{v_{q1(3)}^{(y)}},\frac{v_{q3(4)}^{(y)}}{v_{q1(4)}^{(y)}}\right]\\
\boldsymbol{\Gamma}_{p2}^{\phi x(x)} &= \mathrm{diag}[1,1]\\
\boldsymbol{\Gamma}_{p2}^{\phi y(x)} &= \mathrm{diag}\left[\frac{v_{p3(5)}^{(x)}}{v_{p2(5)}^{(x)}},\frac{v_{p3(6)}^{(x)}}{v_{p2(6)}^{(x)}}\right]\\
\boldsymbol{\Gamma}_{q2}^{\phi x(y)} &= \mathrm{diag}\left[\frac{v_{q2(5)}^{(y)}}{v_{q3(5)}^{(y)}},\frac{v_{q2(6)}^{(y)}}{v_{q3(6)}^{(y)}}\right]\\
\boldsymbol{\Gamma}_{q2}^{\phi y(y)} &= \mathrm{diag}[1,1]
\end{aligned} \tag{A.5}$$

where the superscript T represents the transpose of the vector or matrix, and diag[] represents the diagonal matrix. The parameters ζ_p and ζ_q, as defined in Eq. (A.3), are the correction factors for the Fourier components. The parameters $\widehat{K}_{xp}(j)$ and $\widehat{K}_{yq}(j)$ in Eq. (A.4) are scaling factors introduced for numerical stability. They are defined as follows:

$$\begin{aligned}
\widehat{K}_{xp(j)} &= \begin{cases} -K_{xp(j)} & \text{if } \mathrm{Im}\left(K_{xp(j)}\right) > 0 \\ K_{xp(j)} & \text{if } \mathrm{Im}\left(K_{xp(j)}\right) < 0 \\ 0 & \text{if } \mathrm{Im}\left(K_{xp(j)}\right) = 0 \end{cases}\\
\widehat{K}_{yq(j)} &= \begin{cases} -K_{yq(j)} & \text{if } \mathrm{Im}\left(K_{yq(j)}\right) > 0 \\ K_{yq(j)} & \text{if } \mathrm{Im}\left(K_{yq(j)}\right) < 0 \quad (j = 1,2,3,\ldots,6) \\ 0 & \text{if } \mathrm{Im}\left(K_{yq(j)}\right) = 0 \end{cases}
\end{aligned} \tag{A.6}$$

In the Eq. (A.6), Im(·) represents the imaginary part of the complex number.

Appendix B

The function definitions in Eqs. (42), (50), and (51) are as follows:

$$\mathbf{E}_{n1}^{(\alpha)} = \begin{bmatrix} \mathbf{e}_{n1}^{(\alpha)}(-d) \\ \mathbf{e}_{n1}^{(\alpha)}(d) \end{bmatrix}, \mathbf{E}_{n2}^{(\alpha)} = \begin{bmatrix} \mathbf{e}_{n2}^{(\alpha)}(-d) \\ \mathbf{e}_{n2}^{(\alpha)}(d) \end{bmatrix} \tag{B.1}$$

$$\begin{aligned}
\boldsymbol{\Phi}_{mn1}^{(\beta)} &= o_m \begin{bmatrix} e^{-\mathrm{i}m\pi/2}\boldsymbol{\varphi}_{mn1}^{(\beta)} \\ e^{\mathrm{i}m\pi/2}\boldsymbol{\varphi}_{mn1}^{(\beta)} \end{bmatrix}, \ \boldsymbol{\Phi}_{mn2}^{(\beta)} = o_m \begin{bmatrix} e^{-\mathrm{i}m\pi/2}\boldsymbol{\varphi}_{mn2}^{(\beta)} \\ e^{\mathrm{i}m\pi/2}\boldsymbol{\varphi}_{mn2}^{(\beta)} \end{bmatrix}\\
\boldsymbol{\Lambda}_{mn1}^{(\beta)} &= o_m \begin{bmatrix} e^{-\mathrm{i}m\pi/2}\boldsymbol{\lambda}_{mn1}^{(\beta)} \\ e^{\mathrm{i}m\pi/2}\boldsymbol{\lambda}_{mn1}^{(\beta)} \end{bmatrix}, \boldsymbol{\Lambda}_{mn2}^{(\beta)} = o_m \begin{bmatrix} e^{-\mathrm{i}m\pi/2}\boldsymbol{\lambda}_{mn2}^{(\beta)} \\ e^{\mathrm{i}m\pi/2}\boldsymbol{\lambda}_{mn2}^{(\beta)} \end{bmatrix}
\end{aligned} \tag{B.2}$$

$$\{\widehat{o}_{n1}, \widehat{o}_{n2}\} = \begin{cases} \{1,1\} & \text{if } n = 0, \dfrac{N_\alpha}{2} \\ \{2,2\mathrm{i}\} & \text{if } n = 2,4,6,\ldots,\left(\dfrac{N_\alpha}{2} - 2\right) \\ \{2\mathrm{i},2\} & \text{if } n = 1,3,5,\ldots,\left(\dfrac{N_\alpha}{2} - 1\right) \end{cases} \tag{B.3}$$

where

$$o_m = \begin{cases} 1 & \text{if } m = 0, \dfrac{N_\beta}{2} \\ 2 & \text{if } m = 1,2,3,\ldots,\left(\dfrac{N_\beta}{2}-1\right) \end{cases}$$

$$\begin{aligned} \boldsymbol{\varphi}_{mn1}^{(\beta)} &= \left\{\varphi_{mn(1)}^{(\beta)}, \varphi_{mn(2)}^{(\beta)}, \varphi_{mn(3)}^{(\beta)}, \varphi_{mn(4)}^{(\beta)}\right\} \\ \boldsymbol{\varphi}_{mn2}^{(\beta)} &= \left\{\varphi_{mn(5)}^{(\beta)} \quad \varphi_{mn(6)}^{(\beta)}\right\} \\ \boldsymbol{\lambda}_{mn1}^{(\beta)} &= \left\{\lambda_{mn(1)}^{(\beta)}, \lambda_{mn(2)}^{(\beta)}, \lambda_{mn(3)}^{(\beta)}, \lambda_{mn(4)}^{(\beta)}\right\} \\ \boldsymbol{\lambda}_{mn2}^{(\beta)} &= \left\{\lambda_{mn(5)}^{(\beta)}, \lambda_{mn(6)}^{(\beta)}\right\} \end{aligned} \tag{B.4}$$

$$\begin{aligned} \varphi_{mn(j)}^{(\beta)} &= \widehat{\varphi}_{mn(j)}^{(\beta)} \times \begin{cases} \left(\sigma_{m1(j)} - \sigma_{m2(j)}\right)\cos k_{\alpha n} d & \text{if } n = 0,2,4,\ldots,\dfrac{N_\alpha}{2} \\ \left(\sigma_{m1(j)} + \sigma_{m2(j)}\right)\sin k_{\alpha n} d & \text{if } n = 1,3,5,\ldots,\left(\dfrac{N_\alpha}{2}-1\right) \end{cases} \\ \lambda_{mn(j)}^{(\beta)} &= \widehat{\lambda}_{mn(j)}^{(\beta)} \times \begin{cases} \left(\sigma_{m2(j)} - \sigma_{m1(j)}\right)\cos k_{\alpha n} d & \text{if } n = 2,4,6,\ldots,\dfrac{N_\alpha}{2} \\ \left(\sigma_{m2(j)} + \sigma_{m1(j)}\right)\sin k_{\alpha n} d & \text{if } n = 1,3,5,\ldots,\left(\dfrac{N_\alpha}{2}-1\right) \end{cases} \end{aligned} \tag{B.5}$$

where $j = 1,\ 2,\ 3,\ldots,6,$ and

$$\begin{aligned} \widehat{\varphi}_{mn(j)}^{(\beta)} &= \frac{\mathrm{i}K_{\beta m(j)}}{\left(k_{\alpha n}^2 - K_{\beta m(j)}^2\right)\sqrt{\zeta_m \zeta_n l d}}, \widehat{\lambda}_{mn(j)}^{(\beta)} = \frac{k_{\alpha n}}{\left(k_{\alpha n}^2 - K_{\beta m(j)}^2\right)\sqrt{\zeta_m \zeta_n l d}} \\ \sigma_{m1(j)} &= \mathrm{e}^{\mathrm{i}\left(K_{\beta m(j)} - \hat{K}_{\beta m(j)}\right)d}, \sigma_{m2(j)} = \mathrm{e}^{-i\left(K_{\beta m(j)} + \hat{K}_{\beta m(j)}\right)d} \end{aligned} \tag{B.6}$$

$$\mathbf{I} = \begin{bmatrix} 1 & 0 \\ 0 & -1 \end{bmatrix} \tag{B.7}$$

$$\begin{aligned} \boldsymbol{\chi}_{n1}^{(\alpha)} &= \mathrm{diag}\left[\mathrm{i}K_{\alpha n(1)}, \mathrm{i}K_{\alpha n(2)}, \mathrm{i}K_{\alpha n(3)}, \mathrm{i}K_{\alpha n(4)}\right] \\ \boldsymbol{\chi}_{n2}^{(\alpha)} &= \mathrm{diag}\left[\mathrm{i}K_{\alpha n(5)}, \mathrm{i}K_{\alpha n(6)}\right] \\ \boldsymbol{\xi}_{n1}^{(\alpha)} &= \mathrm{i}k_{\alpha n} \cdot \mathrm{diag}[1,\ 1,\ 1,\ 1] \\ \boldsymbol{\xi}_{n2}^{(\alpha)} &= \mathrm{i}k_{\alpha n} \cdot \mathrm{diag}[1,\ 1] \end{aligned} \tag{B.8}$$

where

$$\begin{aligned} &\beta = y,\ l = a,\ d = b,\ n = r,\ m = q \text{ if } \alpha = x; \\ &\beta = x,\ l = b,\ d = a,\ n = s,\ m = p \text{ if } \alpha = y \end{aligned}. \tag{B.9}$$

Data availability

Data will be made available on request.

References

[1] M.E. Biancolini, C. Brutti, L. Reccia, Approximate solution for free vibrations of thin orthotropic rectangular plates, J. Sound. Vib. 288 (1–2) (2005) 321–344.

[2] S. Sellam, K. Draiche, Y. Tlidji, et al., A simple analytical model for free vibration and buckling analysis of orthotropic rectangular plates, Struct. Eng. Mech. Int'l J. 75 (2) (2020) 157–174.

[3] M. Nefovska-Danilovic, N. Kolarevic, M. Marjanović, et al., Shear deformable dynamic stiffness elements for a free vibration analysis of composite plate assemblies–Part I: theory, Compos. Struct. 159 (2017) 728–744.

[4] M. Chauhan, P. Mishra, S. Dwivedi, et al., Development of the dynamic stiffness method for the out-of-plane natural vibration of an orthotropic plate, Appl. Sci. 12 (11) (2022) 5733.

[5] Ö. Civalek, Free vibration analysis of symmetrically laminated composite plates with first-order shear deformation theory (FSDT) by discrete singular convolution method, Finite Elem. Anal. Des. 44 (12–13) (2008) 725–731.

[6] X. Liu, J.R. Banerjee, Free vibration analysis for plates with arbitrary boundary conditions using a novel spectral-dynamic stiffness method, Comput. Struct. 164 (2016) 108–126.

[7] I. Park, U. Lee, A generic type of frequency-domain spectral element model for the dynamics of a laminated composite plate, Compos. Struct. 172 (2017) 83–101.

[8] T. Kim, U. Lee, Exact frequency-domain spectral element model for the transverse vibration of a reangular Kirchhoff plate, J. Sound. Vib. 492 (2021) 115812.

[9] F. Shirmohammadi, S. Bahrami, Dynamic response of circular and annular circular plates using spectral element method, Appl. Math Model 53 (2018) 156–166.

[10] I. Park, T. Kim, U. Lee, Frequency domain spectral element model for the vibration analysis of a thin plate with arbitrary boundary conditions, Math. Probl. Eng. 2016 (1) (2016) 9475397.

[11] V. Sarvestan, H.R. Mirdamadi, M. Ghayour, Vibration analysis of cracked Timoshenko beam under moving load with constant velocity and acceleration by spectral finite element method, Int. J. Mech. Sci. 122 (2017) 318–330.

[12] Z.J. Wu, F.M. Li, Y.Z Wang, Study on vibration characteristics in periodic plate structures using the spectral element method, Acta Mech. 224 (5) (2013) 1089–1101.

[13] M. Boscolo, J.R. Banerjee, Dynamic stiffness formulation for composite Mindlin plates for exact modal analysis of structures. Part I: theory, Comput. Struct. 96 (2012) 61–73.

[14] N. Kolarevic, M. Nefovska-Danilovic, M. Petronijevic, Dynamic stiffness elements for free vibration analysis of rectangular Mindlin plate assemblies, J. Sound. Vib. 359 (2015) 84–106.

[15] J.R. Banerjee, S.O. Papkov, X. Liu, et al., Dynamic stiffness matrix of a rectangular plate for the general case, J. Sound. Vib. 342 (2015) 177–199.

[16] C. Zhang, G. Jin, T. Ye, et al., Harmonic response analysis of coupled plate structures using the dynamic stiffness method, Thin-Walled Struct. 127 (2018) 402–415.

[17] Y. Xing, G. Li, Y. Yuan, A review of the analytical solution methods for the eigenvalue problems of rectangular plates, Int. J. Mech. Sci. 221- (2022) 221, https://doi.org/10.1016/j.ijmecsci.2022.107171.

[18] H. Guo, X. Zhuang, T. Rabczuk, A deep collocation method for the bending analysis of Kirchhoff plate[J]. arXiv preprint arXiv:2102.02617 (2021).
[19] E. Samaniego, C. Anitescu, S. Goswami, et al., An energy approach to the solution of partial differential equations in computational mechanics via machine learning: concepts, implementation and applications[J], Comput. Methods Appl. Mech. Eng. 362 (2020) 112790.
[20] X. Zhuang, H. Guo, N. Alajlan, et al., Deep autoencoder based energy method for the bending, vibration, and buckling analysis of Kirchhoff plates with transfer learning[J], Eur. J. Mech.-A/Solids 87 (2021) 104225.
[21] S. Kshirsagar, K. Bhaskar, Accurate and elegant free vibration and buckling studies of orthotropic rectangular plates using untruncated infinite series, J. Sound. Vib. 314 (3–5) (2008) 837–850.
[22] Y.F. Xing, B. Liu, New exact solutions for free vibrations of thin orthotropic rectangular plates, Compos. Struct. 89 (4) (2009) 567–574.
[23] X. Liu, J.R. Banerjee, An exact spectral-dynamic stiffness method for free flexural vibration analysis of orthotropic composite plate assemblies–Part I: theory, Compos. Struct. 132 (2015) 1274–1287.
[24] X. Liu, J.R. Banerjee, An exact spectral-dynamic stiffness method for free flexural vibration analysis of orthotropic composite plate assemblies–Part II: applications, Compos. Struct. 132 (2015) 1288–1302.
[25] O. Ghorbel, J.B. Casimir, L. Hammami, et al., Dynamic stiffness formulation for free orthotropic plates, J. Sound. Vib. 346 (1) (2015).
[26] Z. Wang, Y. Xing, An extended separation-of-variable method for free vibrations of orthotropic rectangular thin plate assemblies[J], Thin-Walled Struct. 169 (2021) 108491.
[27] S. Papkov, J. Banerjee, Dynamic stiffness formulation for isotropic and orthotropic plates with point nodes, Comput. Struct. (2022), https://doi.org/10.1016/j.compstruc.2022.106827.
[28] E. Reissner, The effect of transverse shear deformation on the bending of elastic. plates, 1945.
[29] R.D. Mindlin, Influence of rotatory inertia and shear on flexural motions of isotropic. elastic plates, 1951.
[30] S. Kshirsagar, K. Bhaskar, Free vibration and stability analysis of orthotropic shear-deformable plates using untruncated infinite series superposition method[J], Thin-Walled Struct. 47 (4) (2009) 403–411.
[31] D. Shi, Z. Zhuang, T. Zhang, Free vibration analysis of orthotropic rectangular Mindlin plates with general elastic boundary conditions[C], //, in: INTER-NOISE and NOISE-CON Congress and Conference Proceedings. Institute of Noise Control Engineering 249, 2014, pp. 1477–1485.
[32] M.R. Bahrami, S. Hatami, Free and forced transverse vibration analysis of moderately thick orthotropic plates using spectral finite element method[J], J. Solid Mech. 8 (4) (2016) 895–915.
[33] B. Liu, Y. Xing, Exact solutions for free vibrations of orthotropic rectangular Mindlin plates, Compos. Struct. 93 (7) (2011) 1664–1672.
[34] B. Liu, Y.F. Xing, J.N Reddy, Exact compact characteristic equations and new results for free vibrations of orthotropic rectangular Mindlin plates, Compos. Struct. 118 (2014) 316–321, https://doi.org/10.1016/j.compstruct.2014.07.051.
[35] S.O. Papkov, J.R Banerjee, Dynamic stiffness formulation and free vibration analysis of specially orthotropic Mindlin plates with arbitrary boundary conditions, J. Sound. Vib. 458 (2019) 522–543.
[36] U. Lee, Spectral Element Method in Structural Dynamics, John Wiley & Sons, 2009.
[37] T. Kim, B. Lee, U. Lee, State-vector equation method for the frequency domain spectral element modeling of non-uniform one-dimensional structures, Int. J. Mech. Sci. 157 (2019) 75–86.
[38] Z. Wu, F. Li, G. Zou, A finite/spectral element hybrid method for modeling and band-gap characterization of metamaterial sandwich plates, Materials 16 (3) (2023) 1098.
[39] J.F. Doyle, J.F. Doyle, Wave Propagation In Structures[M], Springer, US, 1989.
[40] N.B.F. Campos, J.R.F Arruda, Modeling Kirchhoff plates with arbitrary boundary conditions by the spectral element method[C], //, in: XII International Symposium on Dynamic Problems of Mechanics (XII DINAME), 2007.
[41] I. Park, U. Lee, D. Park, Transverse vibration of the thin plates: frequency-domain spectral element modeling and analysis[J], Math. Probl. Eng. 2015 (1) (2015) 541276.
[42] T. Kim, U. Lee, Temporal and spatial-domain DFT-based spectral element model for the dynamic analysis of a rectangular Mindlin plate, J. Sound. Vib. 509 (2021) 116220.
[43] Y. Zhou, F. Yao, C. Bai, et al., Bandgap characteristics of periodic mindlin plates under arbitrary boundary conditions via the spectral element method[J], Thin-Walled Struct. 205 (2024) 112370.